AD-A067 198 ARMY MATERIALS AND MECHANICS RESEARCH CENTER WATERTO--ETC F/G 11/2
FRACTURE OF GRAPHITE COMPOSITES UNDER SHOCK LOADING.(U)
DEC 78 E C GOEKE, F A MCCLINTOCK

UNCLASSIFIED AMMRC-TR-78-49 NL

|OF|
AD
A067198

END
DATE
FILMED
6-79
DDC

AMMRC TR 78-49

FRACTURE OF GRAPHITE COMPOSITES UNDER SHOCK LOADING

December 1978

ARMY MATERIALS AND MECHANICS RESEARCH CENTER
Watertown, Massachusetts 02172

The findings in this report are not to be construed as an official Department of the Army position, unless so designated by other authorized documents.

Mention of any trade names or manufacturers in this report shall not be construed as advertising nor as an official indorsement or approval of such products or companies by the United States Government.

DISPOSITION INSTRUCTIONS

Destroy this report when it is no longer needed.
Do not return it to the originator.

DEPARTMENT OF THE ARMY
ARMY MATERIALS AND MECHANICS RESEARCH CENTER
Watertown, Massachusetts 02172

OFFICIAL BUSINESS

POSTAGE AND FEES PAID
DEPARTMENT OF THE ARMY
DOD 314

THIRD CLASS MAIL

UNCLASSIFIED

SECURITY CLASSIFICATION OF THIS PAGE (When Data Entered)

REPORT DOCUMENTATION PAGE

READ INSTRUCTIONS BEFORE COMPLETING FORM

1. REPORT NUMBER: AMMRC-TR-78-49	2. GOVT ACCESSION NO.
3. RECIPIENT'S CATALOG NUMBER	
4. TITLE (and Subtitle): FRACTURE OF GRAPHITE COMPOSITES UNDER SHOCK LOADING	5. TYPE OF REPORT & PERIOD COVERED: Final Report
6. PERFORMING ORG. REPORT NUMBER	
7. AUTHOR(s): Elizabeth C. Goeke and Frank A. McClintock*	8. CONTRACT OR GRANT NUMBER(s)
9. PERFORMING ORGANIZATION NAME AND ADDRESS: Army Materials and Mechanics Research Center, Watertown, Massachusetts 02172, DRXMR-RD	10. PROGRAM ELEMENT, PROJECT, TASK AREA & WORK UNIT NUMBERS: D/A Project: PWD-75-225-27, AMCMS Code: 692000.22.50001
11. CONTROLLING OFFICE NAME AND ADDRESS: U. S. Army Materiel Development and Readiness Command, Alexandria, Virginia 22333	12. REPORT DATE: December 1978
	13. NUMBER OF PAGES: 54
14. MONITORING AGENCY NAME & ADDRESS(if different from Controlling Office): 6pp.	15. SECURITY CLASS. (of this report): Unclassified
	15a. DECLASSIFICATION/DOWNGRADING SCHEDULE

16. DISTRIBUTION STATEMENT (of this Report)

Approved for public release; distribution unlimited.

17. DISTRIBUTION STATEMENT (of the abstract entered in Block 20, if different from Report)

18. SUPPLEMENTARY NOTES

*Massachusetts Institute of Technology, Cambridge, Massachusetts 02139

Published in Journal of Applied Physics, v. 46, November 1975, p. 4671-4673.

19. KEY WORDS (Continue on reverse side if necessary and identify by block number)

Graphite composites
Fracture (mechanics)
Shock mechanics
Computerized simulation

20. ABSTRACT (Continue on reverse side if necessary and identify by block number)

(SEE REVERSE SIDE)

79 04 09 002

DD FORM 1 JAN 73 1473 EDITION OF 1 NOV 65 IS OBSOLETE

403 105

UNCLASSIFIED

SECURITY CLASSIFICATION OF THIS PAGE (When Data Entered)

Block No. 20

ABSTRACT

A previously obtained set of experimental data on the failure of three-dimensional graphite composites under shock loading was examined. The critical event was determined to be fracture in the fiber bundles parallel to the shock direction. Physical considerations, as well as a simple approximate equation and a computer model of the fiber bundle fracture, show rather definitely that for pulse widths less than 0.5 μsec the variability in the strength of the individual fibers is the primary cause of the observed stress-pulse width relationship. The assumptions of the computer model include a static stress concentration around the broken fibers and a fiber strength described by an extreme value distribution.

CONTENTS

	Page
INTRODUCTION	1
MATERIAL DESCRIPTION	1
EXPERIMENTAL DATA	1
FORMULATION OF A MODEL FOR SHOCK DAMAGE	2
DATA FROM THE MODEL	3
CONCLUSIONS	6
APPENDIX A. BACKGROUND MATERIAL	
INTRODUCTION	7
MATERIAL DESCRIPTION	
Three-Dimensional Composites	8
Unidirectional Composites	9
SHOCK LOADING	11
Three-Dimensional Composites	11
Unidirectional Composites	16
NATURE OF SHOCK DAMAGE	18
Three-Dimensional Composites	18
Unidirectional Composites	19
APPENDIX B. MODEL DEVELOPMENT	
A QUALITATIVE DESCRIPTION OF FRACTURE	21
TRADITIONAL DESCRIPTIONS OF SHOCK-LOADING DAMAGE	23
APPENDIX C. MODEL DESCRIPTION	
A MODEL FOR SHOCK DAMAGE	27
DATA FROM THE MODEL	34
ASSESSMENT OF THE MODEL	38
APPENDIX D. COMPUTER PROGRAM FOR FIRST MODEL	45
APPENDIX E. COMPUTER PROGRAM FOR SECOND MODEL	51

INTRODUCTION

The proposed use of graphite composites in missile substructures has created a need for understanding their fracture under shock loading. A set of composite materials has been fabricated and shock loaded by Effects Technology, Inc., under Army sponsorship.[1] The present study formulates a physical theory of dynamic fracture consistent with these tests.

MATERIAL DESCRIPTION

The set of composites consisted of three samples with the following construction. Several layers of conventionally woven graphite fabric in the x-y plane, with z direction graphite fibers between the warp and filling, formed a three-dimensional structure which was filled with phenolic resin SC1008. The yarns used for the fabric and in the z direction are later referred to as fiber bundles. Sample M_ℓ has low fibers (6×10^6 psi or 4.4×10^6 bars) in all directions and a low porosity. Sample M_h differs in that the z direction fibers are high modulus (59×10^6 psi or 4.07×10^6 bars). Sample M_{hp} differs from M_h in that it has about 10% porosity.

EXPERIMENTAL DATA

The samples were shock loaded using magnetic flyer techniques. Mylar and polymethyl methacrylate (PMMA) flyer plates giving approximately square wave pulses of width from 0.2 to 2.0 microseconds were used on specimens of 0.6-centimeter thickness to measure fracture thresholds and attenuation. The impacted specimens were sectioned and polished to determine the fracture thresholds, defined in terms of microscopic damage. Tuler and Graham[1] then converted the flyer velocities and flyer thicknesses at fracture threshold to impact stresses and pulse widths using the fiber bundle and matrix impedances. They also used the attenuation data to compute the stresses at the rear surface at fracture threshold. The stress-pulse width data are plotted in Figure 1 to show the observed failure characteristics. The immediate conclusion from the data is that the stress at fracture threshold varies with the width of the pulse and this relationship is nonlinear. A closer examination of the data leads to the following additional conclusions. Although stress at the fracture plane should best describe material response, one decides that either front face or rear face data can be used since the nature of the time dependence remains essentially the same. Voids do not appear to improve material performance. From the calculated stress in the matrix, there are only small differences between the behavior of the three materials. From the calculated stress in the fiber bundles, the fiber modulus does affect performance; M_ℓ (lower modulus) has a consistently lower impact strength.

In the search for the origin of the time dependence the sectioned and polished specimens were reexamined in more detail and the following qualitative description of the fracture was compiled. All specimens have cracks at the fiber-matrix interface; these were concluded to be fabrication defects. The complex

1. TULER, F. R., and GRAHAM, M. E. *Stress Wave Damage in Advanced Concept Materials.* Effects Technology, Inc., Santa Barbara, CA, Contract DAAG46-71-C-0073, Final Report, AMMRC CTR 72-11, July 1972.

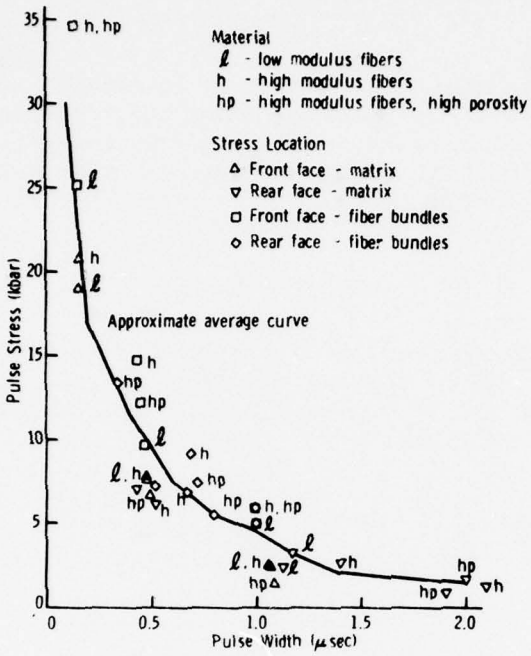

Figure 1. Experimental fracture thresholds.

microstructure of the composites allows many variations in the fracture pattern. Additional cracks in the matrix, fiber breaks in the z direction bundles, and complete separation are the types of damage observed. No significant differences were noted in the fracture patterns in the three materials, only differences in the impact stresses at which phenomena occurred. The sequence of events as stress increased or the pulse lengthened was, first, increasing numbers of cracks in the matrix, then cracks in the fiber bundles, and finally complete separation. The first fiber breaks were isolated or near-neighbor fibers fracturing at locations which might be displaced axially by several fiber diameters. As damage increased these fiber breaks coalesced into a jagged crack.

FORMULATION OF A MODEL FOR SHOCK DAMAGE

Traditional descriptions of shock-loading damage relate the stress and pulse width conditions that give a defined threshold or total fracture. Several such criteria reviewed by Cohen and Berkowitz[2] were examined for applicability to the composites of this study. The power law criterion of Butcher and Tuler,[3] the rate process criterion, and an exponential criterion were found to fit the experimental data well for all three materials. These criteria offer little insight into the mechanism of fracture, however.

2. COHEN, L. J., and BERKOWITZ, H. M. *Time-Dependent Fracture Criteria for 6061-T6 Aluminum Under Stress-Wave Loading in Uniaxial Strain.* Int. J. Fracture Mechanics, v. 7, no. 2, 1971, p. 183-196.
3. TULER, F. R., and BUTCHER, B. M. *A Criterion for the Time Dependence of Dynamic Fracture.* Int. J. Fracture Mechanics, v. 4, no. 4, 1968, p. 431-437.

Formulating a failure mechanism implies examining the materials at the micromechanical level. For composites this means locating the critical element: matrix, fibers, or matrix-fiber interface. For shock loading at room temperature the matrices used are below their glass transition temperatures and thus are elastic, brittle materials. Therefore the matrix is not a good candidate for a source of the time dependence observed in the experimental data. Similar arguments should apply to the fiber-matrix interface. The fiber bundles in the z direction are known from comparison with data from other layups to provide the largest fraction of the strength of these materials. It was therefore concluded that fracture of the fiber bundles was the critical step in the fracture of the composites.

The question then is how a large group of parallel cylindrical elastic bodies (a fiber bundle) of varying strength can show time-dependent fracture. Of the possible sources of a rate effect, i.e., dynamics, quantum mechanics, and thermal motion, the latter two are eliminated by the fact that rate effects are not observed in bare fibers. Turning to dynamics as a source, since the fibers in the bundle are of varying strengths, the arrival of a pulse of a given tensile strength may break only a fraction of the fibers. From each broken fiber a disturbance propagates with the velocity of sound in the material. The propagating disturbance increases the stress on neighboring fibers. Whether this increase leads to a cascade of fiber breaks depends on how high the stress is, on how short the pulse is, and on the fiber strength distribution.

A computer model of the fiber bundles was constructed to calculate the effect of the strength distribution. A one-dimensional array of parallel contiguous fibers is considered along one cross-sectional plane of the fiber bundle. A random number generator is used with the third asymptotic extreme value distribution to generate a fiber strength distribution. This gives the probability ϕ of strength less than S in terms of three parameters:

$$\phi = 1 - \exp\left\{ - \left[\frac{(S-S_\ell)}{(S_0-S_\ell)} \right]^{1/m} \right\} . \qquad (1)$$

The disturbances from broken fibers are assumed to expand by one fiber diameter in each time interval and to immediately assume the static stress distribution around a hole in a plate. The stress on each fiber is calculated at each time interval and compared to its strength. The time for fracture of the bundle is thus found as a function of the strength distribution characteristics and the applied stress. Details are given in the appendixes.

DATA FROM THE MODEL

The first calculation scheme used in the model required calculation times too long for realistic fiber bundle sizes (a thirty-second limitation on an IBM 370 or a two-minute limitation on a Univac 1006 was imposed by the investigators). The experimental fiber bundles contain approximately 10,000 fibers which is a diameter of 100 fibers; thus 100 fiber arrays would simulate the experimental configuration. However, calculations on 20 fiber arrays did show time dependence in the fracture

data motivating further refinement of the model. An alternative calculation scheme was found which allowed at least six runs within the time limit. This was used to study the model.

The first check on the model was the use of the following simple analysis. As a first approximation the fracture time is that required for the disturbances from broken fibers to reach each other's sources. The density of broken fibers is found from the probability of fracture of a fiber for a given pulse strength. For this simple analysis with its assumptions, the fracture time t expressed as a multiple of wave travel time across a fiber d/c is the reciprocal of the probability of fiber fracture:

$$t/(d/c) = 1/\phi \ . \qquad (2)$$

These analytical fracture times are compared to the computer data in Figure 2. The agreement tends to confirm the validity of the model calculations. (It will be seen below that this agreement was somewhat fortuitous.)

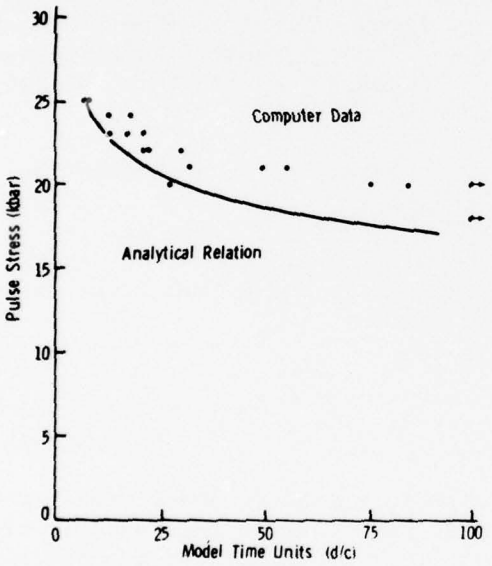

Figure 2. Computer and analytical fracture thresholds. $S_0 = 34$, $S_\ell = 1.0$, $m = 5$.

To facilitate comparison of the computer data with the experimental data, a mean curve was drawn through all the experimental data. Two assumptions were necessary before the comparison could be made: the propagation velocity of the disturbance and the parameters of the fiber strength distribution. Our physical understanding of the mechanism led to the assumption that the disturbance propagates with the shear wave velocity in the material. When this was inserted in the computer model, the model and experimental data have similar pulse width ranges. The fiber strength distribution for the z bundle fibers in the material was not available. Such information for fibers of higher modulus (Celanese 70) was found and parameters for the extreme value description were generated using a technique

described by Matthews, McClintock, and Shack.[4] These parameters were used in the model as a first approximation from which adjustments were made to improve the agreement between the experimental and computer fracture data. Figure 3 shows the experimental mean curve, the computer data which best fits it, and the analytical curve for these parameters. Differences between the analytical and computer data occur at lower values of m where the fiber strength variability is greater. This should have been expected from the cascading of fractures required to stress the remaining fibers to their strengths. The simple analysis neglects such cascading which explains its divergence.

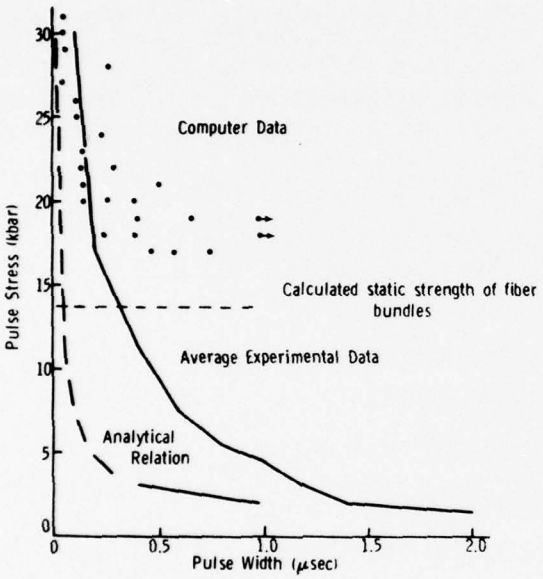

Figure 3. Experimental, computer, and analytical fracture thresholds. $S_0 = 40$, $S_\ell = 1.0$, $m = 1.25$.

The differences between the experimental and computer data led to speculation that the model assumed an incorrect stress distribution around broken fibers. Several other stress distributions were explored but none of them showed as much time dependence as the original one. It was then concluded that this was the best fit possible with the model formulated.

Tuler and Graham[1] calculated the static strength of the fiber bundles to be 13.7 kilobars. They attribute experimental values below this level to compressive wave damage. Although no substantial visual evidence of such damage was seen, a preliminary calculation of static buckling showed that the fiber bundles could buckle under the load pulse conditions. In fact, such buckling could be the explanation of the disparity between model and experimental data at low stress levels and long pulse widths. Further investigation of buckling was beyond the scope of this study.

4. MATTHEWS, J. R., McCLINTOCK, F. A., and SHACK, W. J. *Statistical Determination of Flaw Density in Brittle Materials.* Industrial Liaison Program Report, M.I.T., 1974.

CONCLUSIONS

The critical element in the fracture of three-dimensional graphite composites under shock loading is the fiber bundles in the shock direction. If the observed relationship between stress and pulse width is attributed to the variability in the strength of the individual fibers, it can be modeled by considering disturbances propagating from fibers as they break. The computer model based on these assumptions generates fracture data which are the same order of magnitude and general nature as the experimental data. The interaction of the shock with the material is more complex than assumed in the model. Compressive wave damage is apparently also possible. However, the model shows that the time dependence for pulses of width less than 0.5 μsec can be attributed to the fiber strength variability.

Further details of the computer model and the sample study can be found in the appendixes.

APPENDIX A. BACKGROUND MATERIAL

INTRODUCTION

Composite materials offer possibilities for creative design to the materials engineer. Since they are assembled by technology, their properties can be varied to fit the intended application. The anisotropy and inhomogeneity that are design assets create problems for the materials engineer since his standard analytical tools and laboratory methods are not adequate to deal with them. The development of more sophisticated analytical tools is currently under active study by many workers. An even stronger effort is being applied to the experimental study of composite material properties.

The study described herein concerns one specific aspect of one type of composite material. Dynamic failure of materials is here understood to mean impact by a stress wave rather than simply rapid loading.

Three types of reinforcement fibers have been used in sizable amounts in composite structures: glass, graphite, and boron. The composites studied here contain graphite fibers. This then is a discussion of the shock loading of graphite composites.

Shock loading can be idealized as the impingement on a target of a pulse of maximum stress σ, duration t or Δt, and infinite lateral extent. As far as possible, edge effects are minimized by utilizing a part that is large compared to the wavelength of the pulse. The shape of the pulse depends on the source of the stress wave. Gas guns and other methods where a flyer is thrown at the target result in square pulses. When the stress wave is due to an explosive charge set off on one face of the target, the pulse is approximately triangular. For square pulses the duration is clearly defined. For triangular pulses some convention must be used to measure the duration.

Graphite composites with a great variety of properties are available. The two sets of materials studied here are representative of this range. One is three dimensional with reinforcement in the three mutually perpendicular directions while the other is unidirectional with reinforcement in only one direction. The fibers used as reinforcement range from the lowest modulus to the highest modulus commonly available. Both matrices are in wide use in composite technology.

Prior to this study a body of experimental data had been developed for these materials.[1,5] The question remains whether a failure criterion can be developed which will fit the shock-loading data and link dynamic fracture to static properties.

5. GRAHAM, M. E., and McHENRY, M. R. *Plate Impact Testing of Composites.* Effects Technology, Inc., Santa Barbara, CA, CR-73-139, June 1973.

MATERIAL DESCRIPTION

Three-Dimensional Composites

Two properties of the three-dimensional composites were varied for the study: the fibers in the shock direction and the porosity or void content. The structure used for these composites is a conventional woven fabric in the x-y plane with z direction fibers between the warp and filling. The result is solid fiber when sectioned through the fabric in the x-y plane but shows spaces between fibers in the x-z and y-z planes. After the structure is assembled, it is impregnated with the matrix resin. The properties of the materials are described in Table A-1. All samples contained low modulus fibers in the woven fabric and approximately fifty percent fibers by volume. The matrix resin is a phenolic in widespread use for graphite composites, SC1008.

Filling the fiber structure with resin is difficult because the polymers used are viscous even in the uncured state. In addition, the polymers shrink when cured. Thus the finished product will have some porosity unless careful use of vacuum and pressure is employed. Microscopic examination of the study materials showed that the porosity of M_1 (low modulus fibers, low porosity) and M_2 (high modulus, low porosity) is in the form of cracks in the matrix "cells" of the structure. The porosity of M_3 (high modulus, high porosity) includes completely missing resin in some cells in addition to the cracks.

Both the longitudinal and shear wave velocities in the materials were measured (Table A-2).[1] It should be noted that the modulus of the z direction fibers has a large effect on the longitudinal velocity while the porosity does not affect either wave velocity. This indicates that the fibers are the primary path for the passage of the sound waves. Also reported is a calculated longitudinal velocity based on the z direction fiber modulus and density. These apply to the fibers

Table A-1. THREE-DIMENSIONAL COMPOSITE PROPERTIES

Material	Fibers in z Direction	Fiber Modulus (psi)	Fiber Strength (ksi)	Composite Density	Volume Fraction Voids
M_1 (M_l)	WYB	6×10^6	90	1.256	0.6%
M_2 (M_h)	Thornel 50S	59×10^6	292	1.284	1.5%
M_3 (M_{hp})	Thornel 50S	59×10^6	292	1.17	10.6%

Table A-2. SOUND VELOCITIES IN THREE-DIMENSIONAL COMPOSITES

Material	Longitudinal Wave Velocity (cm/μsec)	Shear Wave Velocity (cm/μsec)	E/ρ
M_1	0.53	0.196	0.56
M_2	1.15	0.185	1.56
M_3	1.14	0.185	1.56

alone and should be modified by using the bundle modulus and density to account for the resin in the fiber bundles which explains the discrepancy between the measured and calculated values.

No other static mechanical properties of the three-dimensional composites were measured.

Unidirectional Composites

One property of the unidirectional composites was varied for the study: the modulus of the reinforcement fibers. The materials were fabricated from prepreg using an autoclave cure. Although the intention was to have identical volume fraction fiber and voids this was not achieved. Table A-3 shows the values measured by acid digestion. The fibers are identified by manufacturer, with Pluton being a 3M product (see Table A-4 for their moduli). The large void content of the Pluton composite has added another factor to the study. Any results must be interpreted with both the differing fiber modulus and this porosity in mind.

Using the "rule of mixtures" with the fiber and matrix properties, theoretical longitudinal tensile moduli and strengths were computed (Table A-4). Tension tests of the materials in the fiber direction using a bow-tie configuration gave modulus values which agree well with the theoretical values but only the Pluton strengths approach theoretical (Table A-5). Failure for the Hercules and Celanese specimens was at the edge of the gage area. This reflects a common difficulty encountered in tension testing composites over six or eight plies thick (these were about twenty plies thick). Transverse tension tests using the same specimen also showed difficulty with the test procedure. The Hercules specimens failed in the gage area while the Pluton and Celanese specimens did not. As shown in Table A-6, addition of the fibers to the resin increases the transverse modulus but decreases the transverse strength of the test specimen. (The resin data is from American Cyanamid and 3M.) Two other sets of mechanical tests completed the mechanical characterization of the material, short beam shear and flexural tests. The shear failure surfaces were rough edges with no distinct evidence of delamination. Discussion with others who have done similar testing indicates these are typical graphite composite short-beam shear failures. Figure A-1 shows the strength versus span relationships measured. It is interesting to postulate that the differing slope for the Pluton material as opposed to the Hercules or Celanese materials can be attributed to the increased void content of the Pluton.

The test configuration of both the tension and flexure specimens was constrained by the size of the plates to be damaged, i.e., the as-received and shock-damaged specimens were to be of the same dimensions. This was of some difficulty for the tension tests but much more serious for the flexural tests. A nonideal four-point loading test configuration was used to obtain the results in Table A-7. The Pluton failures were at the midpoint of the beam and of a tensile nature. The Hercules and Celanese specimens failed under one of the loading points and thus gave inadequate tests. Further research on the test method has not resulted in an adequate method.

One other type of mechanical testing was applied to some of the unidirectional material. A Vibron to measure the loss modulus and storage modulus was

Table A-3. FIBER AND VOID CONTENT OF UNIDIRECTIONAL COMPOSITES

Fiber	Volume Fraction Fiber	Void Content (%)	Volume Fraction Resin (computed)	Density (grams/cc)
Pluton	0.585	5.7	0.358	1.318
Hercules	0.475	0.05	0.524	1.563
Celanese	0.515	1.0	0.475	1.604

Table A-4. RULE OF MIXTURE TENSILE PROPERTIES OF UNIDIRECTIONAL COMPOSITES

	Fiber Modulus (psi)	Fiber Strength (ksi)	Composite Modulus (psi)	Composite Strength (ksi)
Fiber				
Pluton	6×10^6	120	3.70×10^6	73.5
Hercules	$50\text{-}60 \times 10^6$	250-325	26.4×10^6	141.2
Celanese	70×10^6	300	36.3×10^6	158.9
Matrix				
BP907	0.53×10^6	9.28		

Table A-5. MEASURED TENSILE PROPERTIES OF UNIDIRECTIONAL COMPOSITES

Fiber	Modulus (psi)	Strength (ksi)	Elongation (%)
Pluton	3.90×10^6	75.7	2.09
Hercules	25.6×10^6	66.8	0.25
Celanese	35.9×10^6	62.7	0.17

Table A-6. MEASURED TRANSVERSE TENSILE PROPERTIES OF UNIDIRECTIONAL COMPOSITES

Reinforcing	Modulus E (psi)	Strength (ksi)	Elongation (%)
Fiber			
Pluton	1.17×10^6	1.45	0.10
Hercules	1.12×10^6	5.52	0.54
Celanese	0.88×10^6	3.06	0.35
Matrix			
BP907	0.53×10^6	9.28	-

available. It will accommodate only samples of two or three plies. Such samples were fabricated from Hercules prepreg. The peaks in the curves measured on these samples indicate that the matrix is a rubber-modified epoxy. However, when the peak associated with the rubber is shifted to the frequency applicable to shock loading, it is still above room temperature. Therefore, the matrix will be an elastic material under shock-loading conditions.

The mechanical properties of the unidirectional materials indicate that they are average or typical materials.

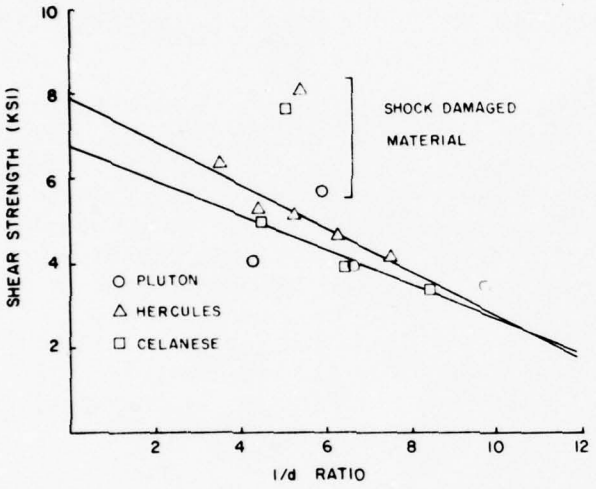

Figure A-1. Short beam shear strength of unidirectional composites.

Table A-7. MEASURED FLEXURAL PROPERTIES OF UNIDIRECTIONAL COMPOSITES - FOUR-POINT LOADING

Reinforcing Fiber	Modulus E (psi)	Strength (ksi)	Elongation (%)
Pluton	2.08×10^6	80.8	21.6
Hercules	7.36×10^6	90.9	17.5
Celanese	11.97×10^6	84.4	19.5

SHOCK LOADING

Two characteristics of the materials under shock-loading conditions were measured: fracture thresholds and attenuation.

Three-Dimensional Composites

All measurements on the three-dimensional composites were made with magnetic flyer plate assemblies. These result in square pulses with the width of the pulse equal to twice the thickness of the flyer. The height of the pulse, i.e., its peak stress, is determined by the velocity of the flyer and therefore by the electromagnetic charge which drives the flyer.

Two types of fracture threshold measurements were made: compressive wave and tensile wave damage. For the compressive wave shots the specimen was backed with a second piece of the test material. The pulse due to the flyer traveled

through the specimen as a compressive wave and on into the backup. For the tensile wave shots the back surface of the specimen was free. The pulse traveled through the specimen as a compressive wave, was reflected from the back surface, and traveled back through the specimen as a tensile wave.

In fracture threshold measurements a series of specimens is impacted with pulses of varying heights. The specimens are examined and categorized as to the amount of damage. The examination is done both macroscopically and microscopically. For the microexamination the specimen is sectioned in the x-z or y-z plane, in the pulse direction, and polished. Most investigators set up arbitrary qualitative amounts of damage as the fracture thresholds or failure points. Some have used quantitative measurements of damage but this involves large amounts of laborious work.

All impacted fracture threshold specimens were 250 mils thick. Three flyer thicknesses were used: 60 mils, 30 mils, and 10 mils; that is approximately 1/4, 1/8, and 1/25 of the specimen thickness. Flyer velocities between 0.40 and 0.006 centimeter per microsecond were used. (This is a stress range of 30 kilobars to one kilobar.) The impacted specimens were categorized qualitatively as to macroscopic damage, then sectioned and categorized qualitatively as to microscopic damage. Figure A-2 shows the fiber damage thresholds and matrix damage thresholds determined for each flyer thickness on each material. The obvious conclusion from this data is that fracture of the materials is a function of both the impact velocity of the flyer and the thickness of the flyer. Further examination shows that neither the modulus of the z direction fibers nor the porosity of the specimen has a large effect on the resistance of the material to shock loading.

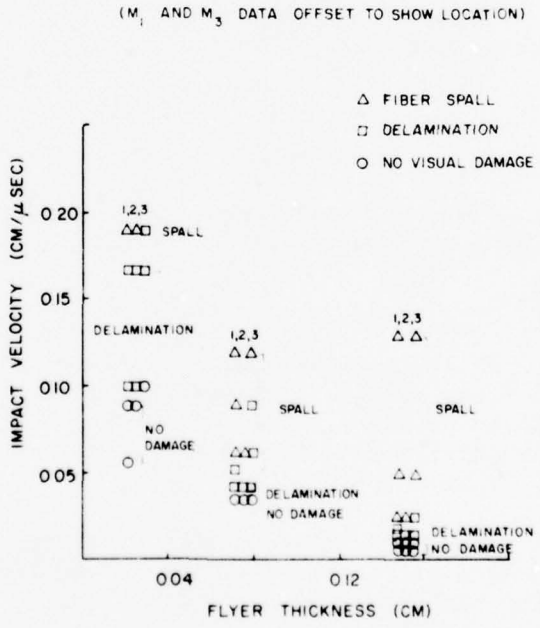

Figure A-2. Fracture thresholds.

Two types of attenuation measurements were made on the three-dimensional composite materials: stress wave attenuation using quartz gages and micromechanical behavior using streak camera photography. In the stress wave technique a quartz gage attached to the rear surface of the specimen records the stress wave after it has passed through the specimen. This was done for three thicknesses: about one third, one half, and the thickness of the fracture threshold specimens. The measurements were taken with two flyer velocities which bracket the threshold velocities. The resulting data is shown in Figure A-3.

To gain further insight into the mechanism of attenuation as measured by these data, Effects Technology normalized the gage stress and the fiber bundle thickness. The normalized stress is the ratio of the back surface stress to the input stress. The normalized bundle thickness is the ratio of the wave transit time to the input pulse length. The resulting curves (Figure A-4) show the effect of flyer thickness. Since the velocity of the pulse is different in the fiber bundles and in the matrix, the wave transit time is different in the bundles and in the matrix. When the normalized thickness differences between matrix and fiber bundles (Figure A-5) are plotted, a set of curves for each flyer thickness is also produced.

The micromechanical measurements using streak camera photography look more closely at the response of the fiber bundles and matrix to the stress pulses. The data consisted of free surface velocities for each constituent and the differences in wave velocities. Attenuation description from this data consists of one set of flyer conditions. The noteworthy result (see Figure A-6) is that at the thicknesses of the threshold specimens the differences in the free surface velocities are not large fractions of the velocities.

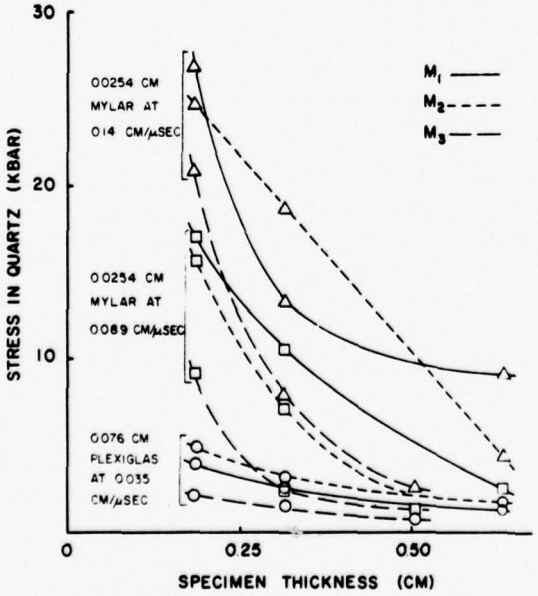

Figure A-3. Stress wave attenuation in three-dimensional composites.

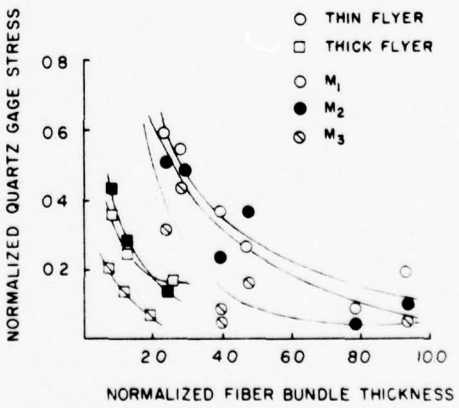

Figure A-4. Normalized attenuation in three-dimensional composites.

In order to examine the data more closely, Effects Technology computed the stress at the back surface from the free surface velocities. This was normalized as before (division by the input stress) and plotted as a function of the normalized specimen thickness (Figures A-7 and A-8). Note that for the fiber bundles all the data for a material fell on a single curve regardless of flyer thickness while for the matrix the thin flyer and thick flyer data required separate curves. The straight lines of the matrix data were the result of the lack of further data points to define the shape of the curve. It is quite likely that curves similar to those for the fiber bundles would be better descriptions of material behavior.

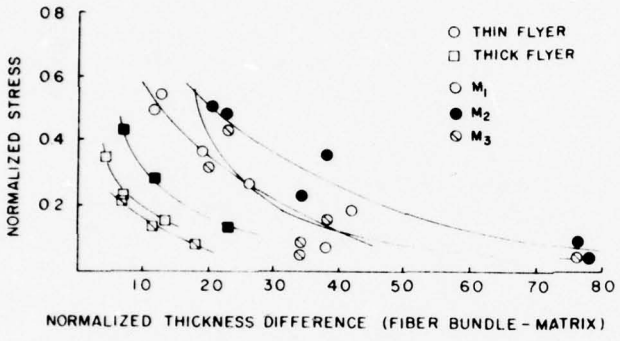

Figure A-5. Differences between fiber bundle and matrix attenuation.

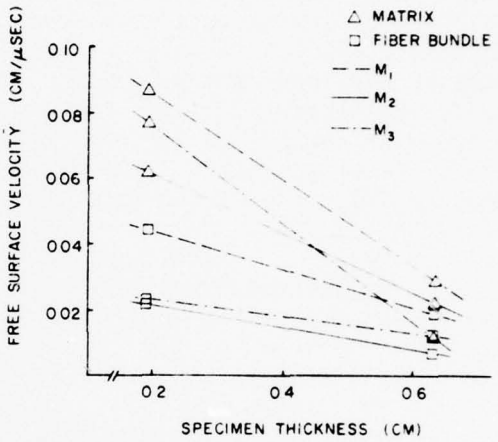

Figure A-6. Attenuation data from streak camera measurements of three-dimensional composites.

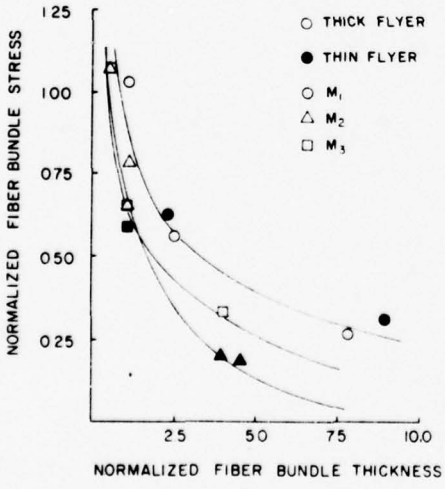

Figure A-7. Normalized fiber attenuation data.

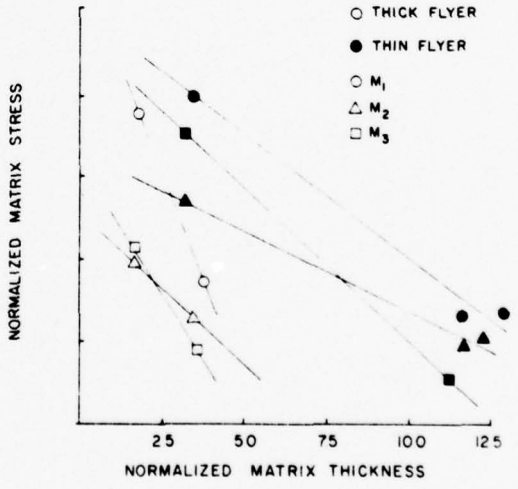

Figure A-8. Normalized matrix attenuation data.

From the streak camera data, Effects Technology computed the stress a quartz gage should measure. These values are compared with the measured quartz gage stresses of the previous set of experiments in Figure A-9. The lack of agreement indicates that some of the assumptions made in the calculations are erroneous. Effects Technology attributes these differences to the spreading of the wave as it passes through the specimen, i.e., the nonplanarity of the wave front.

Effects Technology draws several conclusions from the attenuation data. They state that attenuation depends strongly on fiber modulus, giving a doubling of attenuation rate for a tenfold change in modulus. They qualify this by noting that spreading of the pulse because of the differing velocities in the matrix and fiber bundles causes a larger decrease in stress. They state that porosity increases attenuation. The stress reduction is the same for varying porosity but the normalized thickness necessary for this reduction decreases with increasing porosity.

The attenuation studies show that the stress pulse is modified in passing through the materials. Thus the impact stresses and pulse widths at initial impact are not the stresses and widths which apply when the tensile damage occurs. Effects Technology calculated the rear surface stresses using the attenuation information with the initial impact data. Although these are not the conditions at the damage location, they are a better approximation of such conditions. The resulting curves can be linearized by using a log-log plot (Figure A-10). This is, however, an insensitive means of examining the data and the differences between the materials no longer are evident. Quantitatively the curves drawn to fit the data state that the pulse stress-pulse width relationship is $\ln\sigma = A - \ln t$.

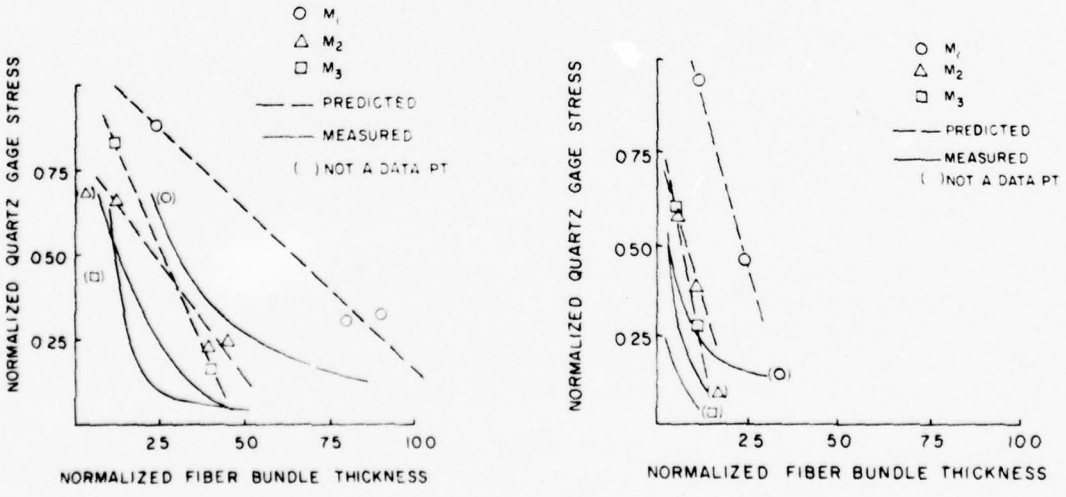

Figure A-9. Predicted and measured attenuation in three-dimensional composites.

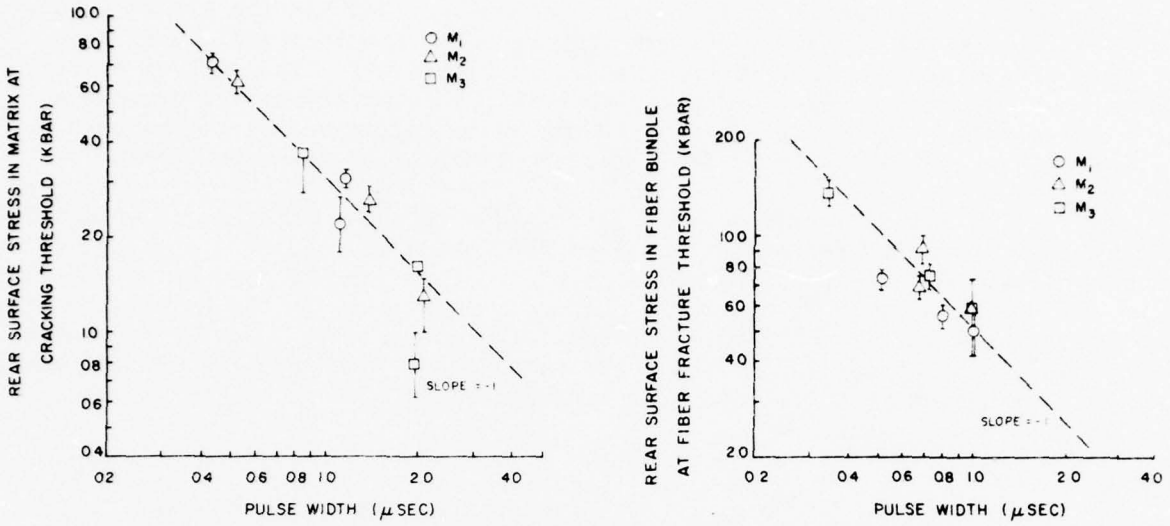

a. Matrix

b. Fiber Bundle

Figure A-10. Rear surface stress-pulse width relation.

Unidirectional Composites

In addition to the fracture threshold and attenuation measurements made on the unidirectional materials, large plates of the materials were shock damaged for post-test mechanical characterization.

Because the unidirectional composites were shock loaded transverse to the fibers their strengths were much smaller than those of the three-dimensional composites. The threshold levels were at the bottom of the range of magnetic flyer techniques. In an effort to improve the quality of the data, contact explosive experiments were also run. The data from all threshold shots is shown in Figure A-11. Some crossply Hercules samples were also tested; these were identical to the Hercules unidirectional samples except for layup. The resulting data is compared in Figure A-12.

The limited amount of fracture threshold data makes conclusions difficult to draw. With square pulses the three unidirectional materials appear to have the same threshold. The threshold for triangular pulses appears slightly higher but still shows no differences among the materials. The puzzling aspect is the lack of any indication that the fracture stress depends on the pulse length.

The attenuation experiments consisted of an initial triangular stress pulse of about two kilobars peak being applied to varying thickness specimens. The resulting data is shown in Figure A-13. It is quite evident that the Hercules unidirectional and crossply materials show the same behavior. The Celanese and Pluton materials show a large degree of scatter that make the assumption of linearity less firm. The increase in attenuation from material to material can be correlated with volume fraction of fiber (see Table A-3).

The damage conditions for the damage plates are given in Table A-8. They were chosen to be fractions of the threshold values to be able to follow the progress of damage.

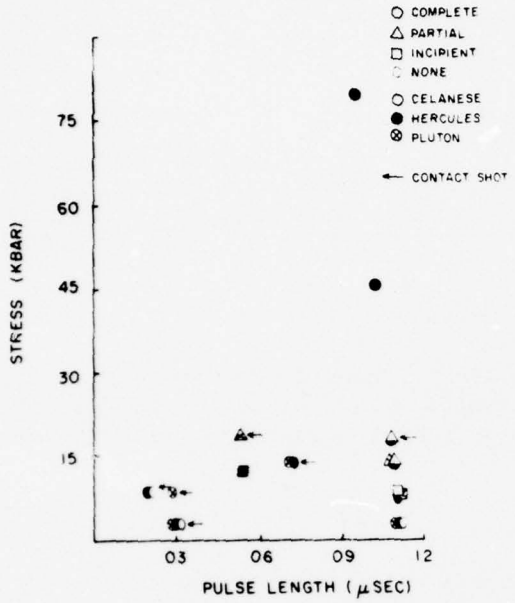

Figure A-11. Fracture thresholds of unidirectional composites.

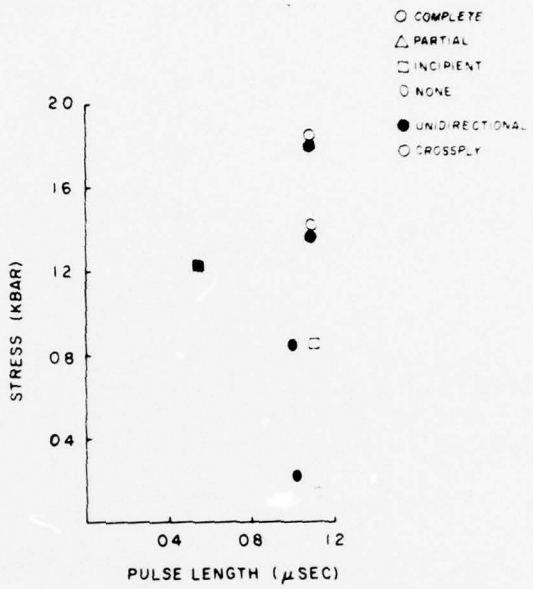

Figure A-12. Fracture thresholds of Hercules fiber material square pulses.

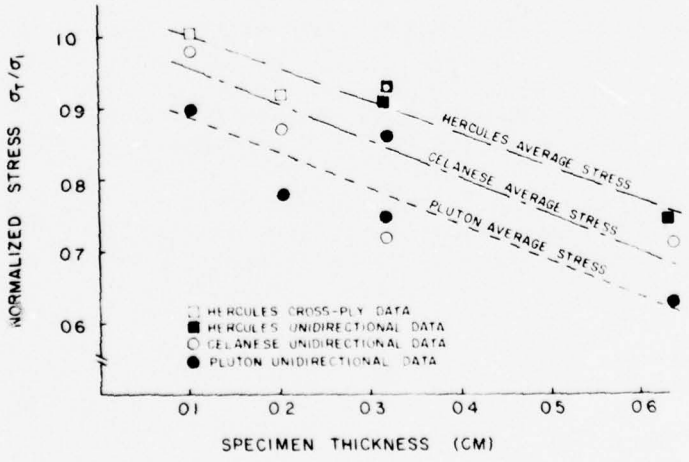

Figure A-13. Stress wave attenuation in unidirectional composites.

Table A-8. DAMAGE CONDITIONS FOR LARGE PLATES

Test Condition		
Pulse Height (kbar)	Duration (μsec)	Specimen
1.84	0.53	PD-7
1.43	0.71	HD-3 HD-9 HD-10 HD-11 CD-11 CD-12 CD-13 PD-5 PD-12 PD-13 PD-14
0.88	0.28	HD-1 HD-2 HD-8 CD-4 CD-5 CD-9 CD-10 PD-6 PD-11
0.28	0.32	HD-4 HD-5 HD-6 HD-7 CD-6 CD-7 CD-8 PD-8 PD-9 PD-10

NATURE OF SHOCK DAMAGE

The examination of the damaged specimens after impact determined when damage occurred but did not provide a sufficiently detailed description of where and how it occurred. The mounted and polished specimens were received from Effects Technology and examined in greater detail.

Three-Dimensional Composites

A preliminary survey of the three-dimensional composite samples led to the establishment of categories of damage. Each sample was then evaluated and its damage classified (Table A-9). As a result of this, some conclusions were drawn.

1. All samples have cracks at the interface between the matrix and the fibers. These cracks can be assumed to be the result of fabrication.

2. No high modulus, high void (M_3) samples have longitudinal cracks in the matrix.

3. For high modulus, low void (M_2) samples no damage to the longitudinal fibers occurs with a flyer velocity of 0.089 centimeter per microsecond or less.

4. For the other two samples (M_1 and M_3) damage to the longitudinal fibers does not correlate with flyer velocity. Broken longitudinal fibers do not occur below a velocity of 0.042 centimeter per microsecond. Above this level they do not necessarily occur.

These observations indicate the difficulty in assigning a fracture level to a composite material where a multitude of defects are possible and damage can occur in many ways. The sequence of events that lead to failure is not obvious from these observations.

The information in Table A-9 was used to determine whether any of the observed damage can be attributed to the compressive wave. Shots employing only compressive waves were compared with tensile wave shots of the same or similar flyer velocities. There was no consistent difference in the damage observed when

Table A-9. DETAILED DESCRIPTION OF SHOCK-LOADING DAMAGE OF THREE-DIMENSIONAL COMPOSITES

	Shot	Longitudinal Fibers A	B	C	D	Transverse Fibers A	E	Resin F	B	G	Flyer Thickness (mils)	Flyer Velocity (cm/μsec)
a. Material M_1 - Low Modulus, z Direction Fibers	2546		x			x		x	x		10	0.19
	2929		x				x		x	x	60*	0.13
	2633			x	close	x		x			10†	0.10
	2635	x					x	x	x		10	0.089
	2524		x		1/3	x			x	x	30	0.052
	2545	x					x	x	x		30*	0.042
	2531			x	1/3		x	x	x	x	30†	0.042
	2520		x			x		x	x		30	0.035
	2516		x			x		x	x		60	0.0175
	2544		x			x			x		60†	0.0145
	2521	x				x		x	x		60†	0.0145
	2923		x			x		x	x		60	0.10
b. Material M_2 - High Modulus, z Direction Fibers	2554			x	1/3	x		x	x		10*	0.167
	2548			x	1/3	x		x	x		10	0.167
	2931		x	x		x		x			30	0.130
	2606			x	1/3		x	x	x		10†	0.100
	2607	x					x	x	x		10	0.089
	2550		x			x		x			30†	0.042
	2534	x				x		x			30†	0.042
	2541	x					x	x			30	0.035
	2931			x	1/6	x		x		x	60	0.025
	2532	x				x			x		60†	0.0145
	2553	x				x		x			60*	0.0145
	2875	x					x	x	x		60	0.010
c. Material M_3 - High Modulus Fibers, High Void Content	2907			x		x		x		x	10	0.19
	2722		x	x	close		x	x			10	0.167
	2755		x	x		x		x			10*	0.167
	2932			x	1/2		x	x			60	0.130
	2724		x			x		x			10†	0.100
	2744			x	close	x		x		x	30	0.042
	2751		x			x		x			30*	0.042
	2726		x			x		x			30†	0.035
	2916		x		1/6	x		x			60	0.025
	2745	x				x		x		x	60	0.0145
	2750		x			x		x			60*	0.0145
	2922	x				x		x			60†	0.010
	2725		x			x		x			60	0.006

*Compressive wave only
†Threshold as defined by ETI

Damage Code: A - no damage
B - longitudinal cracks
C - broken fibers
D - distance from edge
E - some cracks
F - interface cracks
G - edges blown away

only a compressive wave travels through the specimen and when the compressive wave is followed by a tensile wave. Therefore, there is no evidence that any of the observed damage is due to the compressive wave.

Unidirectional Composites

The unidirectional fracture threshold specimens were sectioned and polished both parallel and perpendicular to the fibers. Only the magnetic flyer threshold specimens were available for examination. Several conclusions were drawn from the examination. Damage occurs at lower stresses in the transverse sections than in the longitudinal sections, thus cracks develop first orthogonal to the fibers

and later parallel to the fibers. Damage consists of both wide and narrow cracks of varying lengths. In general, they are in the matrix material and not of straight path. Although some cracks are in the shock direction and at varying angles to the shock direction, the majority are perpendicular to the shock direction.

There are no significant differences in the appearance of the materials, indicating that neither fiber modulus nor porosity have a significant effect on the appearance of failure. The holes or voids in the Pluton material do not appear compacted.

The damage plates were cut and examined in several ways. The sectioned and polished pieces showed no evidence of damage, i.e., no cracks in the materials. Acid digestion measurements of the fiber volume fraction and void content indicate that shock loading has not changed these quantities. Short-beam shear tests measured consistently higher values than those measured on the as-received materials (see Figure A-1). These differences are larger than can be explained by the change in surface condition which occurred when the damaged plates were prepared for shock loading.

APPENDIX B. MODEL DEVELOPMENT

A QUALITATIVE DESCRIPTION OF FRACTURE

The majority of current work on shock loading of homogeneous materials quantitatively describes the shock damage by measuring the void or pore distribution in the damaged material. This task is more difficult for composite materials because of the crack and void patterns present in undamaged material.

For this study, the characteristics of the "as-received" materials were based on the micrographs provided by Effects Technology. As a result a detailed qualitative description of the fracture process was assembled but no quantitative data collected. The microcracks, apparently due to fabrication, are predominantly in the z direction. In the damaged materials there are additional cracks in the x-y plane of the composite (at fracture threshold). The majority of these x-y cracks extend from one z bundle to another. In the z direction fiber bundle damage is not necessarily in contiguous fibers or at the same location along the fibers.

Several quantitative descriptions or models of the fracture were explored. One was a calculation of the energy lost by the pulse in passing through the sample. The calculated pulse stresses and widths based on both the fracture threshold and attenuation data were used with several assumptions: the pulse is square; the pulse velocity is equal to the longitudinal sound velocity in the composite; and the pulse energy is given by the product of the height P, width t, and velocity v ($E = Ptv$). The values thus calculated show only small differences between the pulse energies at the front face and the pulse energies at the back face. In fact, these differences are apparently smaller than experimental error. The available experimental techniques are thus not sufficiently accurate to make this a valid means of describing fracture.

The above rough energy calculation led to exploring what possible processes absorb the energy during the passage of the pulse through the material. Matrix material such as the phenolic of the three-dimensional composites is an interconnected network of long polymer chains. A typical structure for the phenolic was found using Lenz,[6] and the necessary bond breakage to fracture the structure was postulated. The number of bonds which would have been broken if all the energy lost by the pulse went into bond breakage was calculated from the above pulse energy losses. The calculated number was several times the structure fracture number. It was concluded that energy is absorbed by rearrangement, vibration, and many other processes besides bond breakage when the matrix fractures.

Many theoretical analyses of fracture processes predict crack velocities which are related to sound velocities in the materials. The observed cracks in the three-dimensional composites were used to calculate crack velocities in the materials. Three assumptions were required: a crack propagates only while the location is acted on by the pulse; the crack propagates across one matrix "cell;" and the pulse width at the tensile plane is the rear surface pulse width. Three

6. LENZ, R. A. *Organic Chemistry of Synthetic High Polymers.* Interscience, New York, 1967, p. 128-133.

TRADITIONAL DESCRIPTIONS OF SHOCK-LOADING DAMAGE

Most investigators of material response under impulsive loads of high intensity and short duration have treated the materials as a continuum. They assemble a body of experimental data and then postulate a condition for fracture which fits it. The experimental data consists of the stress and pulse width at the impact surface and perhaps the stress and pulse width at the rear surface, which for this study was linked to damage at an interior location in the specimen. None of these stresses and pulse widths are the conditions at the damage location but the latter approach them more closely. Cohen and Berkowitz[2] have summarized the relationships between stress and pulse width which have been developed in this manner.

The simplest of these is a critical stress criterion. For the materials of this study, such a criterion is not adequate since failure depends on both the pulse stress and the pulse width. Stress gradient criteria have been proposed in several forms; these can not be applied to this data because square pulses whose gradients are not easily measurable were used in the experiments.

The criterion suggested by Butcher and Tuler[3] is of a form applicable to this data. It was examined in some detail. The criterion assumes there is a base stress below which no damage occurs and that the relationship between the peak stress and the pulse width is a power function, i.e., $\sigma-\sigma_0 = a\Delta t^b$. The calculated stress-pulse width data for both impact and rear surface stress provided by ETI were examined for fit to this relationship. An exponential plot program was used for the examination. The program is provided by Hewlett-Packard with their programmable calculator. The correlation parameter describes the least-squares fit of the data and has values between zero and one, with one indicating perfect correlation. The parameters describing the curves are functions of the units of stress and should be used only for comparison purposes when the same units have been used. Figure B-1 shows the impact stress at matrix threshold. The correlation parameter value of 0.99 indicates that the data fits this description well. It should be noted that the equation constants and the matrix differs for M_3, the high porosity material. Thus, it can be concluded from this that voids affect the performance of the material. The fiber threshold data was analyzed in several ways as shown in Figure B-2. The correlation was insensitive to choice of zero stress, i.e., stress below which no damage occurs. This is probably due to the use of only three data points for each curve. One fact holds for both impact and rear surface thresholds: M_1, the low modulus fiber material, has differing equation constants from those of M_2 and M_3. Thus the modulus of the reinforcement fibers affect the shock resistance of the material. The Butcher-Tuler criterion[3] gives a good description of the behavior of these materials; however, it offers little insight into why these materials fail.

Failure criteria, utilizing the impulse applied to the material, have been formulated in several ways. These are quite useful for pulse shapes other than square, where peak stress or pulse width are not as well defined. Because the impulse data for the study materials was not available these criteria were not examined.

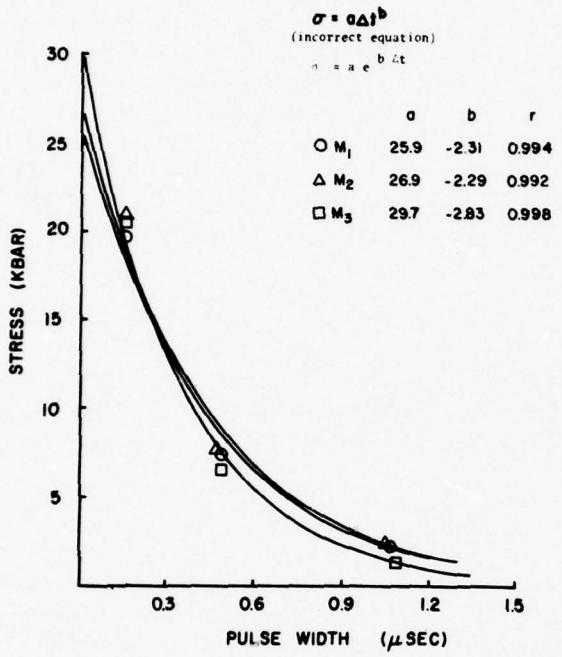

a. Matrix Impact

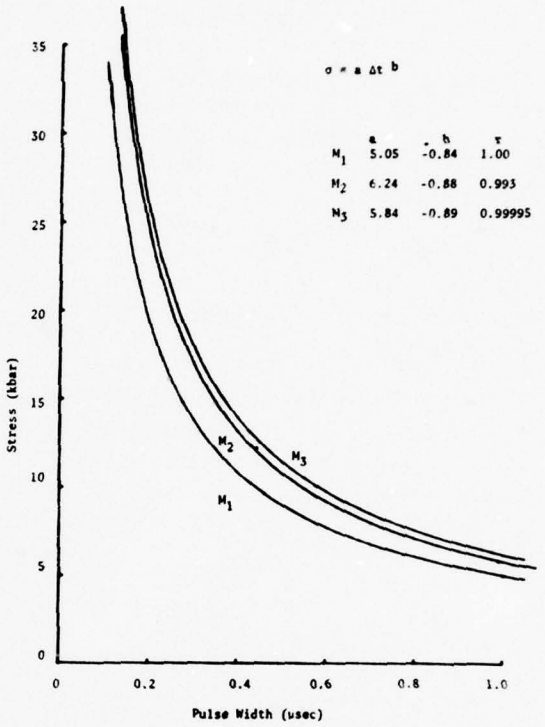

b. Fiber Impact

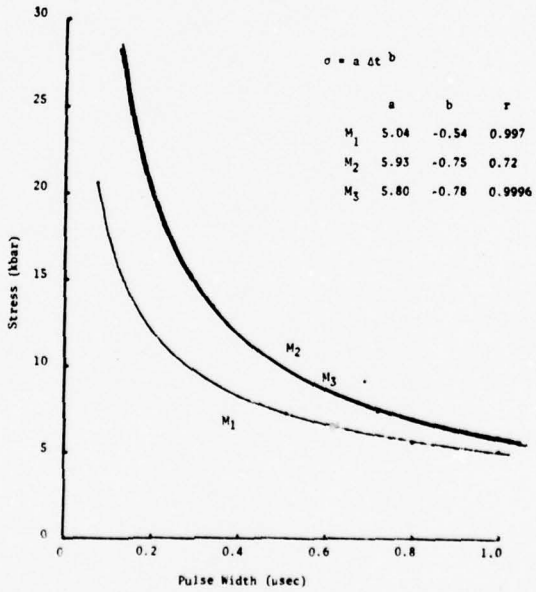

c. Fiber Rear Surface

Figure B-1. Fracture threshold stress.

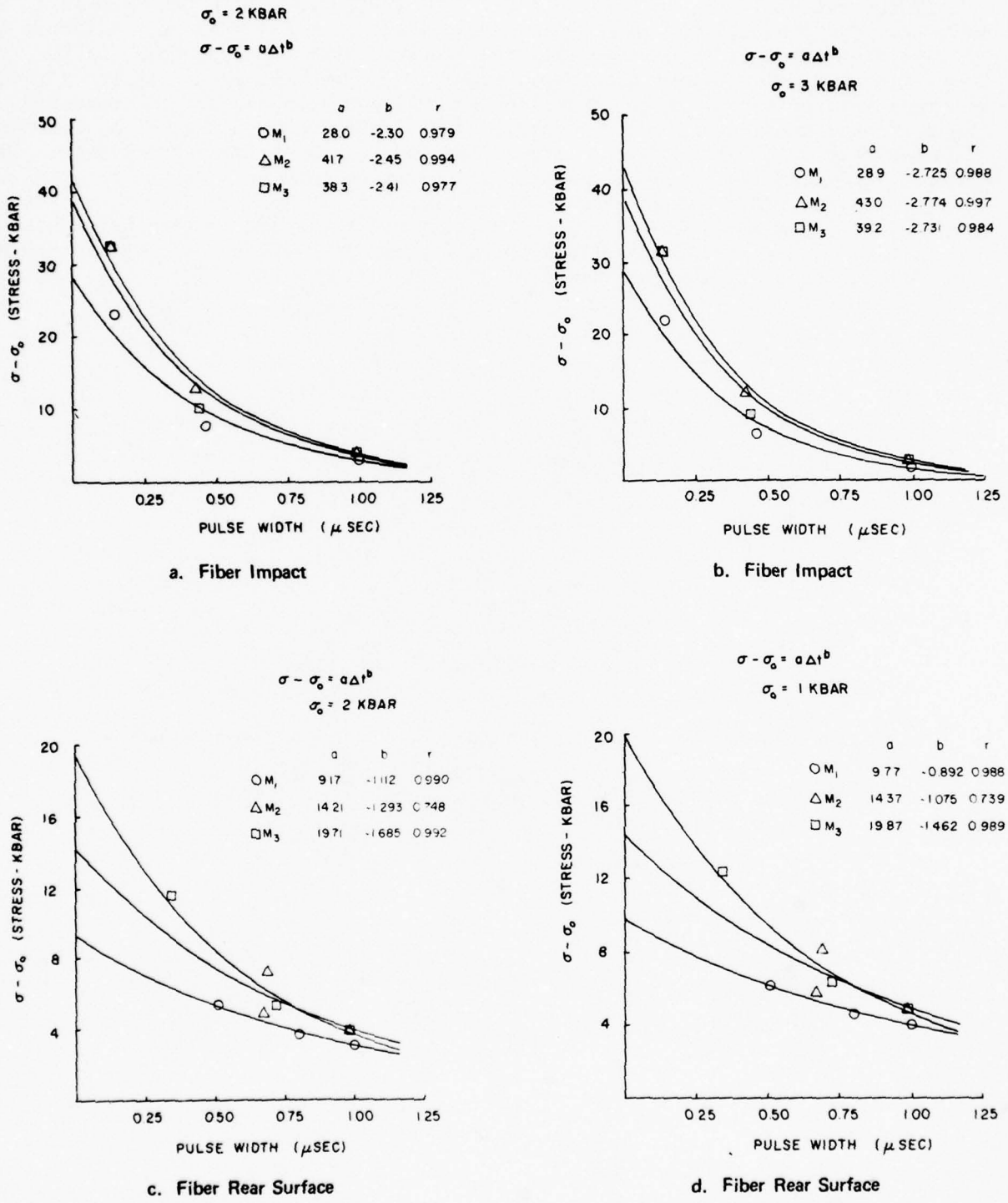

Figure B-2. Fracture threshold stress.

Tuler and Graham[1] concluded at the end of their study that the materials were well described by the rate process criterion: $\sigma = A + B \log t$. A linear plot program was used to examine this relationship with the logarithms of the pulse width obtained before plotting. Figure B-3 shows the matrix impact stress and rear surface stress data. Excellent correlation is shown and the equation constants are consistent with the matrix of M_3 differing from that of M_1 and M_2. Figure B-4 shows the fiber impact stress and fiber rear surface stress data. In general, the correlation is excellent. The equation constants do not clearly differentiate between the material with low modulus z direction fibers, M_1, and those with high modulus fibers, M_2 and M_3. It can therefore be concluded that the rate process criterion describes the observed data well but it does not offer any information as to why this is so.

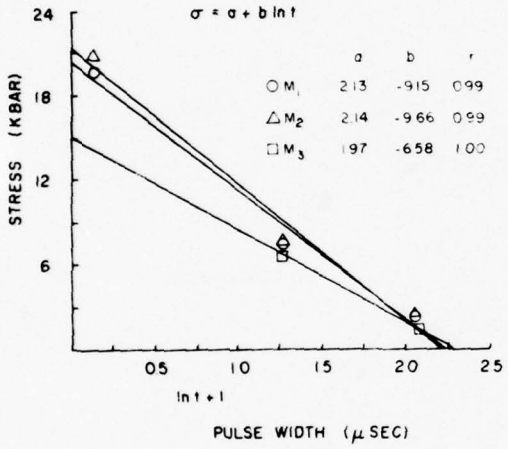

a. Matrix Impact

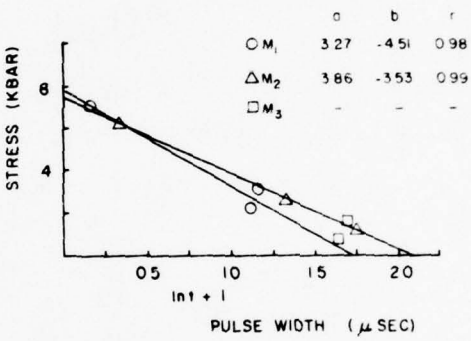

b. Matrix Rear Surface

Figure B-3. Fracture threshold stress.

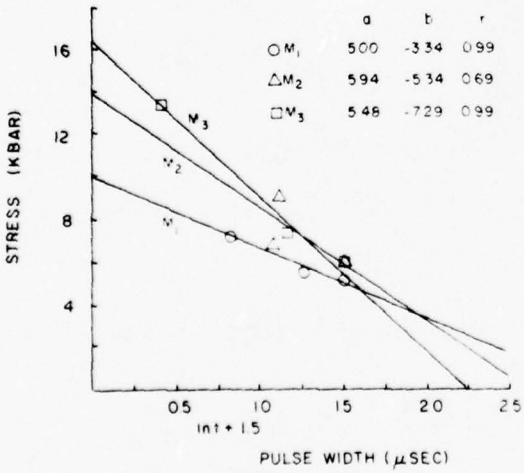

a. Fiber Impact

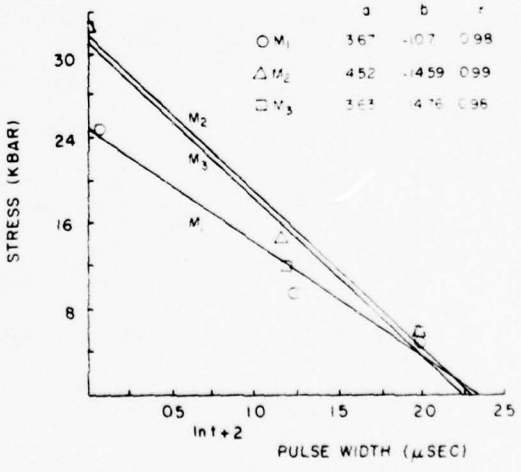

b. Fiber Rear Surface

Figure B-4. Fracture threshold stress.

Army Materials and Mechanics Research Center,
Watertown, Massachusetts 02172
FRACTURE OF GRAPHITE COMPOSITES UNDER
SHOCK LOADING - Elizabeth C. Goeke and
Frank A. McClintock

AD________________

UNCLASSIFIED
UNLIMITED DISTRIBUTION

Key Words

Graphite composites
Fracture (mechanics)
Shock mechanics

Technical Report AMMRC TR 78-49, December 1978, 54 pp -
illus-tables, D/A Project PWD-75-225-27,
AMCMS Code 692000.22.50001

A previously obtained set of experimental data on the failure of three-dimensional graphite composites under shock loading was examined. The critical event was determined to be fracture in the fiber bundles parallel to the shock direction. Physical considerations, as well as a simple approximate equation and a computer model of the fiber bundle fracture, show rather definitely that for pulse widths less than 0.5 μsec the variability in the strength of the individual fibers is the primary cause of the observed stress-pulse width relationship. The assumptions of the computer model include a static stress concentration around the broken fibers and a fiber strength described by an extreme value distribution.

Army Materials and Mechanics Research Center,
Watertown, Massachusetts 02172
FRACTURE OF GRAPHITE COMPOSITES UNDER
SHOCK LOADING - Elizabeth C. Goeke and
Frank A. McClintock

AD________________

UNCLASSIFIED
UNLIMITED DISTRIBUTION

Key Words

Graphite composites
Fracture (mechanics)
Shock mechanics

Technical Report AMMRC TR 78-49, December 1978, 54 pp -
illus-tables, D/A Project PWD-75-225-27,
AMCMS Code 692000.22.50001

A previously obtained set of experimental data on the failure of three-dimensional graphite composites under shock loading was examined. The critical event was determined to be fracture in the fiber bundles parallel to the shock direction. Physical considerations, as well as a simple approximate equation and a computer model of the fiber bundle fracture, show rather definitely that for pulse widths less than 0.5 μsec the variability in the strength of the individual fibers is the primary cause of the observed stress-pulse width relationship. The assumptions of the computer model include a static stress concentration around the broken fibers and a fiber strength described by an extreme value distribution.

Army Materials and Mechanics Research Center,
Watertown, Massachusetts 02172
FRACTURE OF GRAPHITE COMPOSITES UNDER
SHOCK LOADING - Elizabeth C. Goeke and
Frank A. McClintock

AD________________

UNCLASSIFIED
UNLIMITED DISTRIBUTION

Key Words

Graphite composites
Fracture (mechanics)
Shock mechanics

Technical Report AMMRC TR 78-49, December 1978, 54 pp -
illus-tables, D/A Project PWD-75-225-27,
AMCMS Code 692000.22.50001

A previously obtained set of experimental data on the failure of three-dimensional graphite composites under shock loading was examined. The critical event was determined to be fracture in the fiber bundles parallel to the shock direction. Physical considerations, as well as a simple approximate equation and a computer model of the fiber bundle fracture, show rather definitely that for pulse widths less than 0.5 μsec the variability in the strength of the individual fibers is the primary cause of the observed stress-pulse width relationship. The assumptions of the computer model include a static stress concentration around the broken fibers and a fiber strength described by an extreme value distribution.

Army Materials and Mechanics Research Center,
Watertown, Massachusetts 02172
FRACTURE OF GRAPHITE COMPOSITES UNDER
SHOCK LOADING - Elizabeth C. Goeke and
Frank A. McClintock

AD________________

UNCLASSIFIED
UNLIMITED DISTRIBUTION

Key Words

Graphite composites
Fracture (mechanics)
Shock mechanics

Technical Report AMMRC TR 78-49, December 1978, 54 pp -
illus-tables, D/A Project PWD-75-225-27,
AMCMS Code 692000.22.50001

A previously obtained set of experimental data on the failure of three-dimensional graphite composites under shock loading was examined. The critical event was determined to be fracture in the fiber bundles parallel to the shock direction. Physical considerations, as well as a simple approximate equation and a computer model of the fiber bundle fracture, show rather definitely that for pulse widths less than 0.5 μsec the variability in the strength of the individual fibers is the primary cause of the observed stress-pulse width relationship. The assumptions of the computer model include a static stress concentration around the broken fibers and a fiber strength described by an extreme value distribution.

Army Materials and Mechanics Research Center,
Watertown, Massachusetts 02172
FRACTURE OF GRAPHITE COMPOSITES UNDER
SHOCK LOADING - Elizabeth C. Goeke and
Frank A. McClintock

Technical Report AMMRC TR 78-49, December 1978, 54 pp -
illus-tables, D/A Project PWD-75-225-27,
AMCMS Code 692000.22.50001

AD______________

UNCLASSIFIED
UNLIMITED DISTRIBUTION

Key Words

Graphite composites
Fracture (mechanics)
Shock mechanics

A previously obtained set of experimental data on the failure of three-dimensional graphite composites under shock loading was examined. The critical event was determined to be fracture in the fiber bundles parallel to the shock direction. Physical considerations, as well as a simple approximate equation and a computer model of the fiber bundle fracture, show rather definitely that for pulse widths less than 0.5 μsec the variability in the strength of the individual fibers is the primary cause of the observed stress-pulse width relationship. The assumptions of the computer model include a static stress concentration around the broken fibers and a fiber strength described by an extreme value distribution.

Army Materials and Mechanics Research Center,
Watertown, Massachusetts 02172
FRACTURE OF GRAPHITE COMPOSITES UNDER
SHOCK LOADING - Elizabeth C. Goeke and
Frank A. McClintock

Technical Report AMMRC TR 78-49, December 1978, 54 pp -
illus-tables, D/A Project PWD-75-225-27,
AMCMS Code 692000.22.50001

AD______________

UNCLASSIFIED
UNLIMITED DISTRIBUTION

Key Words

Graphite composites
Fracture (mechanics)
Shock mechanics

A previously obtained set of experimental data on the failure of three-dimensional graphite composites under shock loading was examined. The critical event was determined to be fracture in the fiber bundles parallel to the shock direction. Physical considerations, as well as a simple approximate equation and a computer model of the fiber bundle fracture, show rather definitely that for pulse widths less than 0.5 μsec the variability in the strength of the individual fibers is the primary cause of the observed stress-pulse width relationship. The assumptions of the computer model include a static stress concentration around the broken fibers and a fiber strength described by an extreme value distribution.

Army Materials and Mechanics Research Center,
Watertown, Massachusetts 02172
FRACTURE OF GRAPHITE COMPOSITES UNDER
SHOCK LOADING - Elizabeth C. Goeke and
Frank A. McClintock

Technical Report AMMRC TR 78-49, December 1978, 54 pp -
illus-tables, D/A Project PWD-75-225-27,
AMCMS Code 692000.22.50001

AD______________

UNCLASSIFIED
UNLIMITED DISTRIBUTION

Key Words

Graphite composites
Fracture (mechanics)
Shock mechanics

A previously obtained set of experimental data on the failure of three-dimensional graphite composites under shock loading was examined. The critical event was determined to be fracture in the fiber bundles parallel to the shock direction. Physical considerations, as well as a simple approximate equation and a computer model of the fiber bundle fracture, show rather definitely that for pulse widths less than 0.5 μsec the variability in the strength of the individual fibers is the primary cause of the observed stress-pulse width relationship. The assumptions of the computer model include a static stress concentration around the broken fibers and a fiber strength described by an extreme value distribution.

Army Materials and Mechanics Research Center,
Watertown, Massachusetts 02172
FRACTURE OF GRAPHITE COMPOSITES UNDER
SHOCK LOADING - Elizabeth C. Goeke and
Frank A. McClintock

Technical Report AMMRC TR 78-49, December 1978, 54 pp -
illus-tables, D/A Project PWD-75-225-27,
AMCMS Code 692000.22.50001

AD______________

UNCLASSIFIED
UNLIMITED DISTRIBUTION

Key Words

Graphite composites
Fracture (mechanics)
Shock mechanics

A previously obtained set of experimental data on the failure of three-dimensional graphite composites under shock loading was examined. The critical event was determined to be fracture in the fiber bundles parallel to the shock direction. Physical considerations, as well as a simple approximate equation and a computer model of the fiber bundle fracture, show rather definitely that for pulse widths less than 0.5 μsec the variability in the strength of the individual fibers is the primary cause of the observed stress-pulse width relationship. The assumptions of the computer model include a static stress concentration around the broken fibers and a fiber strength described by an extreme value distribution.

APPENDIX C. MODEL DESCRIPTION

A MODEL FOR SHOCK DAMAGE

Examination of the sequence of events leading to failure has shown that, in general, matrix fracture is followed by fiber bundle fracture. It can also be shown that the fibers carry the majority of the load. Thus, in terms of structural integrity, the fiber bundle fracture is the critical event. It was therefore concluded that the most important portion to model was the fiber bundle fracture.

The bundles are composed of large numbers of parallel graphite fibers. The individual fibers are very stiff and almost completely elastic. Compared to textile fibers, there is a great deal of variability in their strength. While for textile fibers a coefficient of variation of 2 percent is usual, values of 12 to 30 percent have been reported for graphite fibers. The question then is how a large group of parallel, cylindrical elastic bodies of varying strengths can show time-dependent fracture.

Under static conditions, when one fiber in a bundle breaks, the load on the bunde is redistributed among the other fibers in the bundle. The model assumes that this redistribution occurs under dynamic conditions. The shock velocities considered here are only slightly higher than sound velocity in the materials. If the redistribution is a disturbance that propagates with the sound velocity in the materials, certain shock pulses will interact with the disturbance. The thesis motivating the model is that if the shock pulse is of the order of the width of the fiber bundle, the fiber strength distribution will be a determining factor in the strength of the bundle. The time dependence of the fiber bundle fracture can be described by studying the sequential fracture of fibers and the resulting propagating stress disturbance seen by neighboring fibers. This involves calculating the stresses on given fibers due to both the pulse and previous fiber failures. Although an individual calculation for this is not difficult, the bookkeeping necessary for the bundle sizes that are appropriate dictated the use of a computer program. This was developed as described below and used to generate failure data. The program can be divided into three parts: the fiber strength calculation, the stress wave propagation calculation, and the display of the resulting fracture data. The development of each of these parts will be discussed in sequence.

Consider the fiber strength distribution, i.e., the variation in the strength of individual fibers within a fiber bundle. The theory motivating the model is that this causes the time dependence in the sample failure and thus a quantitative description of it is essential.

Graphite fibers are observed to fail in a brittle manner; that is, they exhibit no yield and have low fracture elongations. Adequate test techniques have been developed for two configurations: impregnated bundle tests and single fiber tests. Data from the single fiber tests are needed for this application. Because fiber bundles contain thousands of fibers and there are large variabilities in the strengths, hundreds of test specimens are necessary to adequately measure the

strength distribution. Some fiber manufacturers have generated such data in the process of developing their fibers, but the data is not readily available in the open literature. Livermore Laboratories* report that the coefficient of variation of Thornel 50 fibers of unspecified length has been measured to be 12 percent. Modmor fibers in two-inch lengths[8] have been measured to have coefficients of variation between 3.6 and 6.1 percent, with a Gaussian distribution of strengths. The most extensive details on fiber distribution used for this study are given by McMahon and apply to Celanese high modulus fibers.[9] A coefficient of variation of 30 percent was calculated for them as part of the analysis described below.

McClintock and Walter[10] discuss a statistical description of fracture of brittle materials which offers a mathematical expression to insert in the model to describe the fiber strength variability. Their description relates the probability of fracture to a material strength distribution. It employs the asymptotic extreme value function of the third kind. The low strength portion of the distribution is assumed to be described by the polynomial:

$$g(S) = \frac{m}{V_\ell} \frac{(S-S_\ell)^{m-1}}{(S_0-S_\ell)^m}$$

where m is an arbitrary constant while V_ℓ, S_0, and S_ℓ are experimental parameters. The material is assumed to contain a uniform density of flaws. Fracture depends on the flaws. This means that the observed strength distribution is a function of the size of the specimen tested. For bulk material, V_ℓ is the volume of the specimen. For fibers, the dimension of significance is the length, i.e., the number of flaws present is proportional to the length of the test specimen and V_ℓ becomes a length L_ℓ. S_ℓ is the lowest existent strength and $L_\ell(S_0-S_\ell)^n$ taken together are a constant. For part of this study S_0 has been assumed to be the mean fiber strength and S_ℓ the lowest observed strength. Using these assumptions the polynomial has the form:

$$g(S) = \frac{m}{L_\ell} \frac{(S-S_\ell)^{m-1}}{(S_0-S_\ell)^m}$$

The problem now becomes that of finding the values for the experimental parameters and m which best describe the available data. One method is to use the Celanese fiber strength distributions given by McMahon as models for the strength distributions of the fibers used in the specimens. This involves analyzing the Celanese distributions, then assuming the specimen fibers have similar distributions and calculating the parameters using the known specimen fiber strengths.

*CHIAO, T. T., private communication.

8. Technical Bulletin, Morganite Modmor Inc., Costa Mesa, CA.
9. McMAHON, P. E. *Graphite Fiber Tensile Property Evaluation.* ASTM STP 521, 1973, p. 367-389.
10. McCLINTOCK, F. A., and WALTER, R. A. *Mechanics and Statistics of Brittle Crack Initiation.* Res. Mem. 184, to be published.

This has been done and the resulting values are given in Table C-1. The assumption of a higher coefficient of variation for the WYB fibers than for the Thornel 50S fibers is based on the effect of the graphitization process necessary to develop high modulus fibers.

There are several methods of determining the parameter m. If S_ℓ is assumed to be zero (c_v is a small fraction, smaller if S_ℓ is not zero), the coefficient of variation can be shown to be related to m by:

$$c_v = \sqrt{\frac{(2/m)!}{((1/m)!)^2} - 1}$$

Values of c_v and m for this relationship are given in Table C-2. The experimental coefficient of variation data indicate that m should be between 4 and 10 by this criterion. Because the strength distributions are reported to be symmetric by McMahon and others and thus have a skewness of zero, Figure 15.16 of McClintock and Argon[11] gives a value of 3.75 for m.

Another method of describing the strength distribution has been developed by Matthews, McClintock, and Shack.[4] This takes experimental data, orders it, and describes the probability of fiber fracture as a polynomial $\phi(S)$. The material strength distribution g(S) is a function of $\phi(S)$:

$$g(S) = \frac{(d\phi(S)/dS)}{\pi d\ell[1-\phi(S)]}$$

This procedure has been applied to some of the data given by McMahon. A Hewlett-Packard programmable calculator program for polynomial fit was used. A fifth-order polynomial was found to give the best description of $\phi(S)$. From this a fourth-order polynomial for g(S) was found. Figure C-1 shows the polynomial for four sets of fiber data given by McMahon, one is for Modmor I fibers while the others are for Celanese 70 fibers. Also plotted are three curves for the McClintock and Walter polynomial. Values of the parameters were varied to find

Table C-1. CALCULATED FIBER DISTRIBUTION PARAMETERS

Fiber	Strength (mean)	c_v	Lowest Observed Strength S_ℓ
Celanese	248 ksi	0.294	95.7 ksi
WYB	6.3 bars	0.30	0.82 bar
Thornel 50S	20.4 bars	0.25	2.5 bars

Table C-2. THE RELATIONSHIP BETWEEN THE COEFFICIENT OF VARIATION AND THE EXPONENT OF THE EXTREME VALUE DISTRIBUTION

(S_ℓ assumed to be zero)

m	c_v
1	1.00
2	0.52
3.3	.33
4	.28
5	.23
6.67	.18
10	.12
20	.06
100	.01

11. McCLINTOCK, F. A., and ARGON, A. S. *Brittle Failure*, Chapter 13 in Mechanical Behavior of Materials, Addison Wesley, MA, 1966.

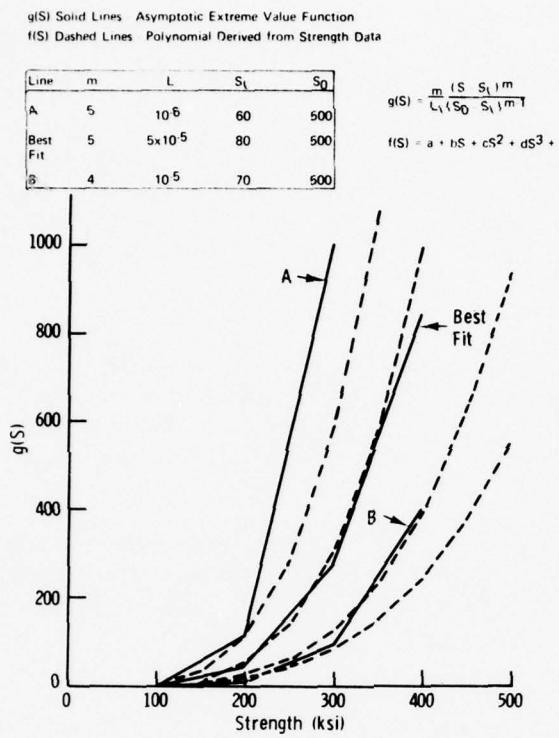

Figure C-1. Polynomials describing fiber strength distributions.

the curve which best fits the experimental data. The form of the McClintock and Walter polynomial is compatible with the form of the model. These parameter values can thus be used to insert experimental fiber strength information in the model. The computer program utilizes the following procedure. A random number generator is used to determine the probability of a given fiber failing. The strength of that fiber is then calculated using:

$$S = S_\ell + (S_0 - S_\ell)(\ln(1-\phi))^{1/m}$$

where ϕ is the probability of failure and S_ℓ, S_0, and m are the parameters which describe the strength distribution. The strength of each fiber in the bundle is calculated and stored.

The stress wave propagation portion of the program was developed from the following analysis. Model the material as a bundle of contiguous parallel fibers. Consider the fibers in the bundle at just one axial location in the sample, i.e., at a given value of the coordinate in the shock direction. This is justified by both the microscopic examination of the samples and the shock wave theory which predicts maximum stress at the plane of first tension. Assume a fiber break occurs instantaneously when the stress on the fiber equals the strength of the fiber. Model the fiber break as a hole. Calculate the stress on each fiber and compare it to the fiber strength as time passes. Figure C-2 is a schematic diagram of the sequence of events.

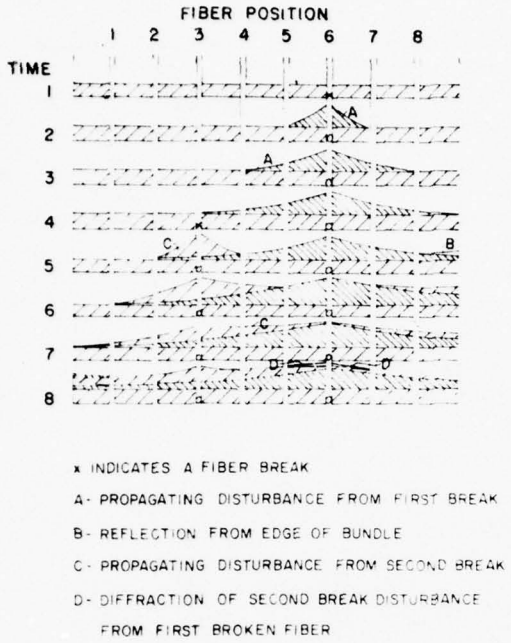

Figure C-2. A schematic diagram of the fiber fracture sequence showing the stress on each fiber at successive times.

The stress at a given location at the current time is labeled SF. Initially the stress on all fibers is the pulse stress, i.e., SF = SP. In the example (Figure C-2) fiber 6 breaks initially, i.e., is weaker than the pulse. As time passes the load previously carried by this fiber is shifted to the neighboring fibers. The wave source strength SW, which is the stress at a given location at the time the fiber at the location breaks, is used to describe the propagating disturbance. The increment in stress on a fiber due to the fracture of another fiber is defined at a specific time as SDT. The total stress on a given fiber at a given time is the stress at the previous time plus the stresses due to the broken fibers, SF = SF + ΣSDT. In Figure C-2 the stress on fiber 3 at time 4 is the pulse stress plus the stress due to the fiber 6 breaking at time 1: SF(3) = SP + SW(1,6)f(IT-ITW). The quantity IT-ITW is the distance between the broken fiber and the fiber of interest since it has been assumed that the disturbance travels one fiber diameter per unit time; f(IT-ITW) is a description of the stress concentration around the hole and is calculated below. Since the assumed bundle width is eight fibers, when the disturbance from fiber 6 reaches fiber 8, it is reflected as shown.

To avoid excessive correlations, only one reflection of any wave at an edge was considered. Therefore, there are three possible paths by which a source can affect a given fiber at a given time. It can be straight line propagation in which case the distance is the difference between the break location and the given location (fiber 4 at time 3). If the disturbance is reflected from the right edge, the distance is the sum of the differences between the maximum number of fibers and the given fiber and broken fiber locations (fiber 8 at time 5). If it is reflected from the left edge, the distance is the sum of the given fiber location minus one and the broken fiber location minus one (fiber 1 at time 8). When the

disturbance from a broken fiber encounters another broken fiber, a hole, it will be diffracted since the broken fiber can sustain no load. The diffraction is an additional wave source. The stress due to the diffraction is that from a source of strength SDT. This is illustrated in Figure C-3. The stress on the surface of the hole can be broken into the sum of the stress on the structure away from the hole and a stress on all surfaces of the structure.

Consider the strength of the disturbance which propagates away from a fiber break. Shock waves are described as pulses of given stress in the shock direction, given length, and uniaxial strain. Model the broken fiber as a circular hole in a plate as shown in Figure C-3. Assume the stress distribution around the hole can be approximated by the steady state distribution. Calculate the increase in stress at point A due to the hole. The configuration is shown in Figure C-4. The load on a fiber at the time when it breaks is uniaxial strain in the x

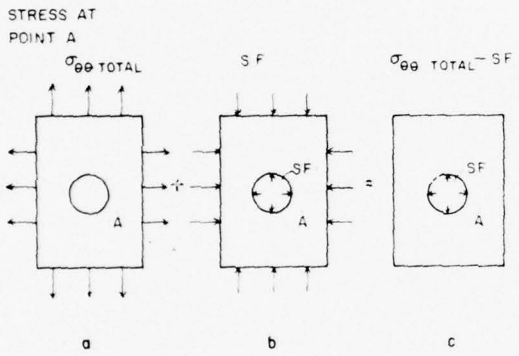

Figure C-3. A stressed plate with a hole.

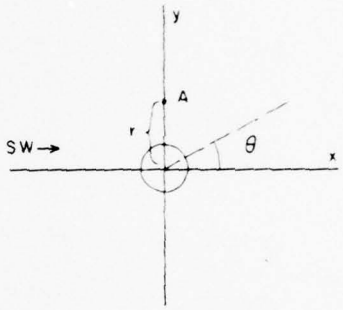

Figure C-4. Geometry for stress concentration calculation.

direction (use polar coordinates with $\theta = 0°$ in the x direction). The prescribed conditions are thus: $\varepsilon_{yy} = \varepsilon_{zz} = 0$. In general $\sigma_{xx} = SW$ while initially $\sigma_{xx} = SP$. The stress in the $\theta = 90°$ direction is $\sigma_{yy} = (\nu/1-\nu)\sigma_{xx}$. Only the stress at point A in the θ direction is needed since this is the axial direction of the fibers. The location has coordinates $(r,90°)$. Calculate the stress due to σ_{xx}, then the stress due to σ_{yy}, and add to find the total stress. Use a second system of coordinates for the latter calculation such that $0^1 = 0 - 90°$; the location has coordinates $(r,0°)$ in this system. Timoshenko and Goodier[12] give the stress distribution around such a hole in a plate as:

$$\sigma_{rr} = (S/2)[1 - (a^2/r^2)] + (S/2)[1 + (3a^4/r^4) - (4a^2/r^2)] \cos 2\theta$$

$$\sigma_{\theta\theta} = (S/2)[1 + (a^2/r^2)] - (S/2)[1 + (3a^4/r^4)] \cos 2\theta$$

where S is the stress on the plate and a the radius of the hole. Using these relationships the stress in the θ direction due to $\sigma_{xx} = SW$ (at $\theta = 90°$) is:

12. TIMOSHENKO, S., and GOODIER, J. N. *Theory of Elasticity*. Oxford Press, New York, 1951, p. 78-80.

$$\sigma_{\theta\theta} = SW[1 + (a^2/2r^2) + (3a^4/2r^4)] .$$

The stress due to $\sigma_{yy} = [\nu/(1-\nu)]SW$ (at $\theta^1 = 0°$)

$$\sigma_{\theta\theta} = (SW/2)[\nu/(1-\nu)][(a^2/r^2) - (3a^4/r^4)] .$$

The sum of these stress is:

$$\sigma_{\theta\theta \text{ total}} = SW [1 + (1/(1-\nu))(a^2/2r^2) + (1-2\nu/(1-\nu))(3a^4/2r^4)] .$$

This is the total stress at point A while the quantity needed is the increase in stress since SDT is defined as the stress increment due to a wave from a fiber fracture. Its value is SDT = $\sigma_{\theta\theta}$ total - SW. The distance r can be expressed in terms of the number of fibers between the hole and the fiber of interest. Including the fiber of interest this distance is r = 2na (see Figure C-5). The stress increment in terms of the number of fibers is therefore:

$$SDT = SW[(1/1-\nu))(1/8n^2) + (1-2\nu/(1-\nu))(3/32n^4)] .$$

Using this description of the stress concentration and the previously described sequence, the computer program does the stress wave propagation analysis.

The concluding portion of the program has several options. The stress on each fiber at each time can be printed. The list of source strengths can be printed. In all cases a fiber break plot that shows the time and location of each break is printed.

To correspond to the experimentally observed fracture data the fiber bundle is defined as failing when a fraction of its fibers has broken. This fracture time is then the width of pulse which would give the defined damage. The fracture data from the model consists of these times.

Appendix D is a listing of the computer program in the form used initially.

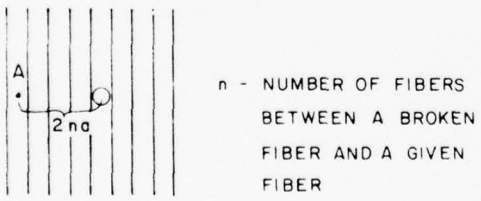

Figure C-5. Geometry of fibers and holes.

DATA FROM THE MODEL

The structure of the computer program is such that the maximum information concerning the progress of the fracture is obtained for a fiber bundle of twenty fibers or less. The initial work was therefore done with a 20-fiber bundle. Table C-3 gives the results of a series of calculations using SDT-A.

$$\text{SDT-A} = \text{SW}\left[\frac{1}{(1-\nu)(8n^2)}\left(1 + \frac{3(1-2\nu)}{4n^2}\right)\right] .$$

For a limited range of pulse strengths the failure time is dependent on the pulse strength. Outside this range the bundle either fails immediately or never fails. Since the fiber bundles in the experimental samples contain 10,000 fibers, computer data for a fiber bundle width of 100 fibers provides better comparison than the smaller bundle. Using the 20-fiber bundle results as a guide, a 100-fiber bundle calculation was made. No difficulty was encountered and a short failure time obtained. However, when a pulse of lower strength was used for the next calculation, it was discovered that the calculation time had been underestimated and such calculations would not be possible within the allotted budget. (A time limit of 30 seconds on an IBM 370 or 2 minutes on a Univac 1006 was imposed by the authors.)

The results of the 20-fiber bundle calculations were examined further. It was noted that the stress increase on the unbroken fibers was less than the stress released by the breaking of the fibers. Thus the model did not approach the static stress distribution at large times. To simplify the description of this discrepancy a model strength distribution was substituted for the random strength distribution. Three fibers in the center of the bundle were assigned a strength less

Table C-3. PULSE STRESS: FRACTURE TIME RELATIONSHIPS FOR THE THREE STRESS INCREMENTS

20-Fiber Bundle, $S_\ell = 0$, $S_0 = 20$, Maximum Time - 20 Model Units

	Pulse Stress (kbar)	Fracture Time (model units)		Pulse Stress (kbar)	Fracture Time (model units)
SDT-A m = 5	10	>19	m = 10	15	>19
	13	>19		16	>19
	15	11		17	12
	18	3		18	3
	20	2		20	<1
SDT-B m = 5	12	>19	m = 10	15	12
	15	7		20	3
	18	5			
	20	4			
	23	2			
SDT-C m = 5	10	>19	m = 10	10	>19
	13	10, >19, >19		13	>19
	15	8		15	>19, >19, >19
	15	13, 9, 7		16	7
	16	4, 6, 5		16	11, 15, 7
	20	3		17	5, 6, 16
	20	3, 3, 4		20	3, 3, 2
	25	2			

NOTE: Grouped data points were run as sets.

than the pulse strength. The remaining fibers were assigned a strength such that they would not break. Results from calculations using this strength distribution are given in Table C-4. A pulse strength of 15 kbar was applied to the bundle thus the stress to be carried by the unbroken fibers is 45 kbar. Since SDT-A adds only 17.8 kbar to the stress on the fibers, it does not satisfy the static asymptote.

Table C-4. EQUILIBRIUM STRESS DISTRIBUTIONS FOR VARYING DESCRIPTIONS OF STRESS CONCENTRATION

20-Fiber Bundle, Maximum Time - 20 Model Units

	Equation	Maximum Stress (kbar) on Fiber Contiguous to Hole	Total Incremental Stress (kbar) on Unbroken Fibers
SDT-A	1	20.2	17.8
-B	2	22.0	23.6
-C	3	29.3	43.0

Stress (kbar) Added by Redistribution at Time 19

	Fiber Position (Number from Hole)								
	1	2	3	4	5	6	7	8	9
SDT-A	5.1	1.6	0.8	0.5	0.3	0.2	0.2	0.1	0.1
-B	6.9	1.8	0.9	0.6	0.4	0.3	0.3	0.2	0.2
-C	14.3	2.8	1.4	0.8	0.6	0.5	0.4	0.4	0.3

An alternate means of evaluating the stress increment is summing the stress on a given fiber and assuming this stress is concentrated at the midpoint of the fiber. This expression will approach the static stress distribution in the limit of long times, i.e.,

$$\int_{n=1/2}^{\infty} SDTdn = \frac{SW}{(1-\nu)}\left[-\frac{1}{8n} - \frac{(1-2\nu)}{32n^2}\right]_{n=1/2}^{\infty} = \frac{SW}{2} .$$

The stress increment is:

$$SDT = -\frac{SW}{(1-\nu)}\left[\frac{1}{8n}\left(1 + \frac{(1-2\nu)}{4n^2}\right)\right]_{n-1/2}^{n+1/2} =$$

$$\frac{SW}{(1-\nu)} \frac{1}{8(n+1/2)(n-1/2)} \left[1 + \frac{(1-2\nu)}{4} \frac{(3n+1/4)}{(n+1/2)^2(n-1/2)}\right] .$$

This can be approximated by:

$$SDT = \frac{SW}{8(1-\nu)} \frac{1}{(n^2-1/4)} .$$

Both the approximate form and the complete form of this were used to calculate equilibrium stress distributions and failure data. These results are given in Tables C-3 and C-4 where

$$\text{SDT-B} = \frac{SW}{8(1-\nu)} \quad \frac{1}{(n^2-1/4)}$$

and

$$\text{SDT-C} = \frac{SW}{8(1-\nu)} \left(\frac{1}{(n+1/2)(n-1/2)}\right)\left[1 + \frac{(1-2\nu)}{4}\left(\frac{1}{(n+1/2)^2} - \frac{1}{(n-1/2)^2}\right)\right] .$$

As can be seen from Table C-4 the third stress increment (SDT-C) approaches the static stress configuration and thus provides a physically consistent description. It was also noted that the third stress increment shows increased time dependence over the first two.

The validity of the time values calculated by the model was questioned. A simple approximation of the fracture time is the reciprocal of the probability of fracture calculated from the extreme value distribution. (If the time for fracture is assumed to be the time for the disturbance from a broken fiber to travel to the next broken fiber, then this time is given by $T = d/c\phi$ where d is the fiber diameter and c is the distrubance velocity in the material.) The model is set up such that the distrubances travel one fiber diameter in each time unit, i.e., $d/c = 1$; thus the time is the reciprocal of the probability. Using

$$\phi = 1 - \exp\left(-(SP-S_\ell/S_0-S_\ell)^m\right)$$

time values were calculated for the conditions used in the model calculations. Figure C-6 compares this approximation with data from the model. Since the data curves lie between the approximation curves, the model calculations are shown to be valid.

Having shown that the model does give a time-dependent pulse strength description that is consistent with long time effects and probability theory, more effort was applied to shortening the calculation method used in the computer program.

The first step taken was to streamline the steps of the calculation as much as possible. One of the changes was to calculate and store a set of influence coefficients instead of calculating each influence coefficient or stress concentration as needed. This did not result in significant improvement. Another was to shift the calculation mode from floating point to integer arithmetic. This also was not adequate.

An alternative method of calculation was developed which had the advantage of a more compact means of storing the wave sources. It employs wave characteristics, i.e., the rays from the sources, and numbers each source along the characteristic as to order of occurrence. A secondary array of the times of initiation of the sources is also generated.

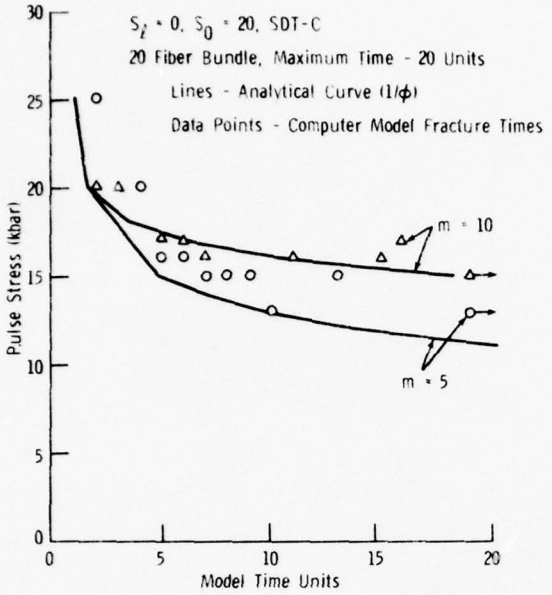

Figure C-6. Comparison of computer and analytical data.

The characteristics are initially assigned the positions of the fibers. Through each position pass two characteristics, one right traveling and one left traveling. The program is unchanged in the preliminary sections. The fiber strengths and the source influence coefficients are calculated and stored. After all the appropriate quantities have been initialized the main calculation begins. As before, the fibers are considered sequentially as time progresses. The array of sources is searched over both characteristics which pass through each fiber. (This is the time reduction since all sources were searched previously.) The contribution of each source is calculated and added to the stress increment. If the fiber has not broken, the stress increment is added to the stress on the fiber. If the fiber has broken, the stress increment is added up and temporarily stored. If the fiber has not broken previously, the stress on it is compared to its strength. If it now breaks, the location becomes a wave source so sources are added to both the characteristics. If the fiber has broken previously, the total stress increment becomes a source on both characteristics. As previously the stress on the fibers is tabulated after each time increment. At the conclusion of the calculation the wave source array is transformed from its characteristic-source number format to the position-time format and tabulated. A fiber break diagram is also printed. The program is given in Appendix E.

The program using this calculation method required acceptable calculation times (less than two minutes). Fracture data for a series of pulse heights were calculated using the strength parameters employed previously. The fracture criterion used was eighty percent of the fibers in the bundle broken. Figure C-7 shows the resulting data. Time dependence is observed with large amounts of scatter in the data for long fracture times. An additional set of data (Figure C-8) was obtained using the strength parameters derived from the Celanese fiber data. Also shown is the curve calculated using the probability function. It should be noted that the probability function shows greater time dependence than the computer data.

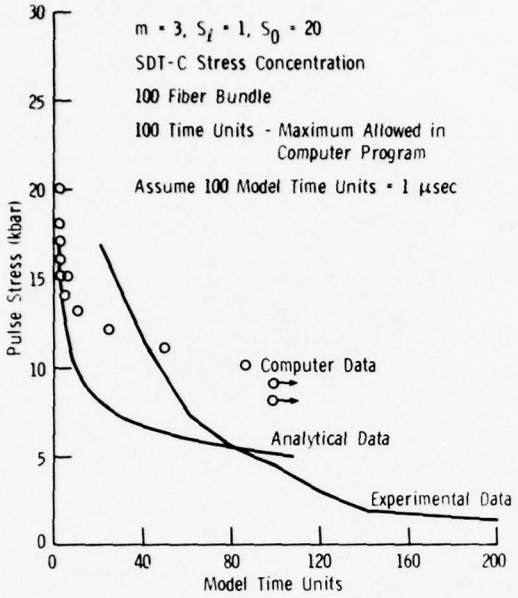

Figure C-7. Computer and analytical fracture data.

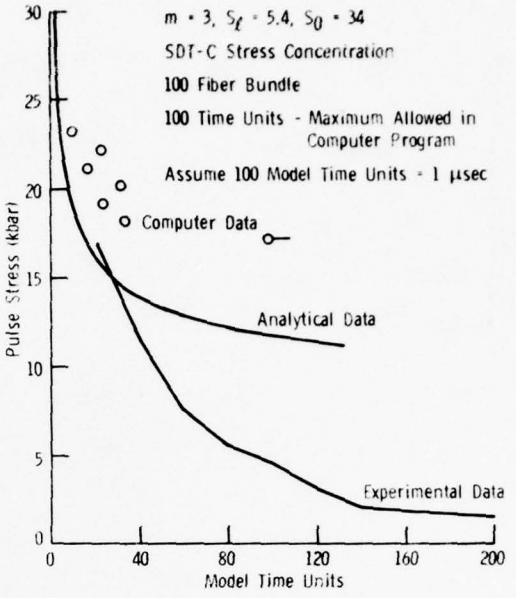

Figure C-8. Computer and analytical fracture data.

ASSESSMENT OF THE MODEL

Comparison of the data from the model with the experimental pulse height-width data requires a definition of the model time unit. The model assumes the disturbance propagates across one fiber diameter during each time unit. The fiber diameter is seven microns. If one assumes the disturbance travels at the longitudinal sound velocity in the material (see Table A-2), 1000 model time units are approximately one microsecond. The model data shows that the pulse height-width relationship exists for less than 100 model time units or approximately 0.1 microsecond for this assumption. Examination of Figure 1 shows that the experimental data gives a pulse height-width relationship for pulse widths between 0.2 and 2 microseconds. If one assumes the disturbance propagates with the shear wave velocity in the material, 100 model time units are approximately one microsecond. With this assumption the model data and the experimental data are in the same range. However, the model data do not fit the experimental data well.

Experimentally, time dependence occurs over a range of almost 20 kbar while the model shows time dependence over a range of 10 kbar or less. Efforts to improve this fit took two directions, parameter adjustment in the strength distribution expression and examination of the stress concentration description. The justification for the parameter adjustment lay in the fact that the fiber strength distributions in the sample were not known.

The examination of the stress concentration began with a literature search. The model assumes that the static stress distribution around a hole under uniaxial strain as described by Timoshenko and Goodier is a good description of the dynamic stress distribution around such a hole. Confirmation of this assumption was sought in the work of others.

Blake[13] discusses the propagation of spherical waves from pressure in a cavity. He found the particle displacement to be:

$$u = \frac{k}{r} e^{-\alpha\tau} \sin \omega_0 \tau$$

where k, α and ω_0 are experimental constants and τ is a reduced time. The time of interest for this case is impact of the pulse on the location for which $f(\tau) \approx 1$. Using:

$$\sigma_r = \frac{E}{(1+\nu)(1-2\nu)} \left\{(1-\nu)\frac{\partial u}{\partial r} + 2\nu\frac{u}{r}\right\}$$

from Hopkins,[14] this displacement results in an inverse square relationship for the stress-distance function which justifies the static assumption of the model.

Hopkins also discusses the disturbance resulting from pressure in a spherical cavity. For the quasi-static case he states that:

$$\sigma_r = -P(a^3/r^3) .$$

He also uses Fourier transforms to analyze the dynamic case. At the conclusion of the analysis he states that at the wavefront:

$$\sigma_r = -(a/r^3)P(0) \quad \textit{and} \quad \sigma_t = (-\nu/1-\nu)(a/r^3)P(0)$$

(assuming the exponent on r has been omitted in his text). If this is a better description of the stress concentration, the model has used a stronger stress concentration than occurs and the damage will propagate more slowly than calculated.

The results of the literature search were therefore ambiguous. It was concluded that investigation of the use of other stress concentration descriptions in the model was warranted.

If the Hopkin's expression is written in the terms used for the model, it becomes:

$$\sigma_r = -(ka^3/r^3)SW \qquad \sigma_t = (-\nu/1-\nu))(ka^3/r^3)SW .$$

The model considers the transverse tension, thus the latter expression was used to develop a new stress increment expression. By the method employed previously and assuming k = 1:

$$SDT\text{-}D = \frac{SW}{8}\left(\frac{\nu}{1-\nu}\right)\left[\frac{n}{(n+1/2)^2(n-1/2)^2}\right] .$$

13. BLAKE, F. G., Jr. *Spherical Wave Propagation in Solid Media.* J. Acoustical Society of America, v. 24, 1952, p. 211-215.
14. HOPKINS, H. G. *Dynamic Expansion of Spherical Cavities in Metals* in Progress in Solid Mechanics 1, Chapter III, Interscience, New York, 1960.

This expression was inserted in the computer program and preliminary fracture data generated with the program. The results are shown in Table C-5. This stress concentration description showed time dependence for a pulse height range of less than 5 kbar. Examination of the fiber break plots showed that there was very little damage propagation in the fiber bundles.

Table C-5. STRESS CONCENTRATION DESCRIPTIONS

(Calculated Using the 100-Fiber Model with $S_o = 20$, $S_\ell = 1.0$, $m = 3$)

Description	Source Distance Dependence	Fracture Data: Pulse Height (kbar)	Fracture Data: Fracture Time (model units)
SDT-E	$1/r^{1.5}$	5	>99
		10	>99
		15	>99
		18	>99
		20	10,17
		23	2
		25	<1
SDT-C	$1/r^2$	9	>99
		10	41,87
		15	6,4
		20	2
SDT-F	$1/r^{2.5}$	10	>99
		20	>99
		25	<1
SDT-D	$1/r^3$	10	>99
		20	>99
		25	<1

Two additional stress concentrations were investigated. They were chosen not on physical grounds but as logical mathematical extensions of the previous trials. The first was:

$$\sigma_t = \frac{\nu}{1-\nu} \frac{ka^{3/2}}{r^{3/2}} SW .$$

This gives a stress increment for the program of:

$$SDT\text{-}E = \frac{SW}{3\sqrt{2}} \left(\frac{\nu}{1-\nu}\right) \left[\frac{1}{(n-1/2)^{1/2}} - \frac{1}{(n+1/2)^{1/2}}\right] .$$

The second description was:

$$\sigma_t = \frac{\nu}{1-\nu} \frac{ka^{5/2}}{r^{5/2}} SW$$

which gives a stress increment of:

$$SDT\text{-}F = \frac{SW}{10\sqrt{2}} \left(\frac{\nu}{1-\nu}\right) \left[\frac{1}{(n-1/2)^{3/2}} - \frac{1}{(n+1/2)^{3/2}}\right] .$$

These stress increments were inserted in the computer program and preliminary fracture data generated. The data shown in Table C-5 was examined to evaluate them. The first expression shows time dependence for a pulse height range of less than 10 kbar and very little damage propagation. The second shows time dependence for less than a 5-kbar range of pulse heights and no damage propagation.

From this investigation it was concluded that the stress concentration description used initially in the model (SDT-C) produces at least as much damage propagation and time dependence as the other feasible alternatives.

The parameter adjustment study concentrated on the value of m, although several sets of experimental parameters were used. For evaluation purposes a criterion was formulated to describe the time dependence of the fracture stress; q is defined as the ratio of the pulse stress which gives a fracture time of eight model units to that for a fracture time of eighty units.

The available computer fracture data which had been generated using the parameters for the Celanese fibers and those projected for the sample fibers were analyzed. For comparison, fracture times were also calculated with these parameter values in the asymptotic extreme value function (the approximation used previously). The resulting values of q are given in Table C-6. It can be seen that decreasing m increases the time dependence (value of q). One also notes that the strength parameters for the sample fibers give about the same time dependence as those for the Celanese fibers when used in the model. Figure C-9 shows the effect of changing the strength parameters on the data.

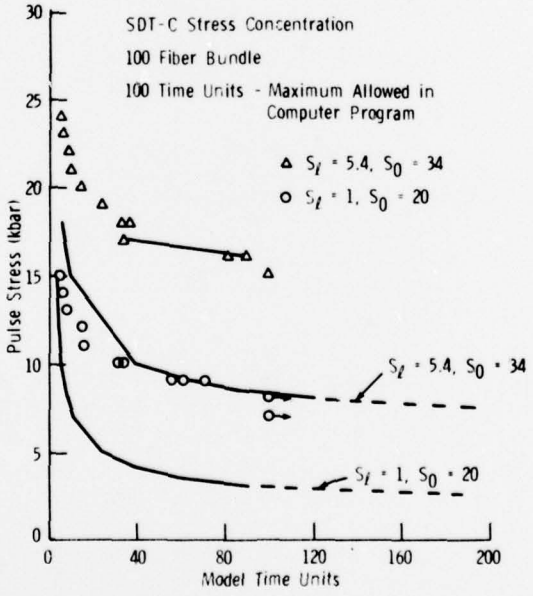

Figure C-9. Computer and analytical fracture data for m = 2.

Table C-6. TIME DEPENDENCE OF PULSE LEVEL RELATED TO THE VALUE OF THE STRENGTH DISTRIBUTION PARAMETER m

Distribution Parameters			Computer Data	Calculated
S_o	S_ℓ	m	q	q
34	5.4	5	1.32	1.45
		3	1.37	1.67
		2	1.38	1.88
		1.5		3.0
		1.2		1.77
20	0	10		1.23
		5	1.4	1.44
20	1	5		1.56
		4		1.67
		3.5		1.85
		3	1.3	2.0
		2.5		2.11
		2	1.44	2.67
		1.5		3.0
		1.3		2.9
		1.2		3.3
		1.1		2.9
		1		2.8
20.4	2.5	2	1.44	

The function used to describe the time dependence is:

$$SP_{t=8}/SP_{t=80} = q$$

The function used to calculate the failure times is:

$$T = \frac{1}{1-\exp[-(S-S_\ell/S_o-S_\ell)^m]} .$$

It is the asymptotic extreme value function used in the computer program to generate the fiber strength distributions.

If the experimental data of Figure 1 in the text is examined, the following value for q represents the time dependence of the experimental data.

$$\frac{SP_{t=0.2\ \mu sec}}{SP_{t=1.0\ \mu sec}} = 3.8 .$$

A means of comparing the time dependence of the experimental data with that from the model was sought. A best fit curve was drawn through the experimental data of Figure I (main text). This represents a first-order approximation of the experimental data. A value of q for the experimental data was calculated from the fracture stress for a pulse width of 0.2 μsec and 1.0 μsec. This is larger than the q for any of the conditions used in the model. Figures C-7 and C-8 compare the mean experimental curve with the analytical curves and the computer data. A time equivalence of 0.01 μsec per model time unit is assumed.

With the mean experimental data available, it appeared of interest to investigate how it fit the probability description. A plot of lnS versus ln(-ln(1-1/T))

gave an approximately linear curve of slope about m = 1.25, thus indicating the experimental data can be represented by the probability description. Examination of Table C-6 shows that q should be high for this m. A set of computer data was generated using S_0 = 40, S_ℓ = 1, and m = 1.25. This was closer to describing experimental observations than any of the previous data as shown in Figure C-10. However, it was noted that the analytical data (from the failure probability) and the computer data do not have similar curves. This is true at lower values of m where the greater strength variability means that the damage propagation in the computer model has a larger effect on the fracture time. It was also noted that a shift of the computer data to longer pulse times and lower stresses would improve the fit but no justification for such a shift was found.

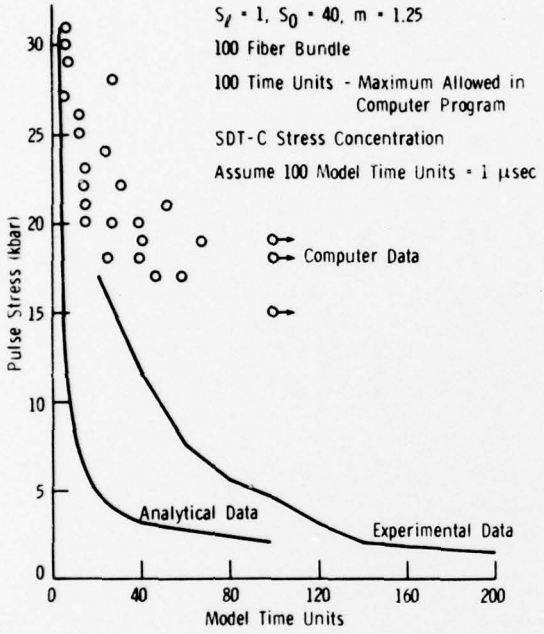

Figure C-10. Computer and analytical fracture data for optimized parameters.

From the foregoing analysis of the parameter effects on the computer fracture data, it was concluded that although the value of the m parameter affects the time dependence of the computer fracture data, the computer data can not by this means be made to fit the experimental data well. Other explanations of the differences were sought.

Tuler and Graham[1] calculated the static strength of the z direction fiber bundles to be 13.7 kbar using the fiber strength and the volume fraction fiber in the bundles (for the high modulus fibers). They attribute the failure at lower strength than this to compressive damage. The visual examination of the polished cross sections of the damaged specimens which was done at the beginning of this study did not show any substantial evidence of such damage. Therefore, in postulating a model, compression was not considered. A cursory examination of the possibility of buckling was in order at this juncture.

The fibers and the fiber bundles are to be considered as columns under compression. Using the strength of materials description of the critical load for buckling, a critical column length for a given load can be calculated. If the column is assumed to have fixed ends, the critical load expression is:

$$P = \frac{4\pi^2 EI}{L^2} .$$

As a preliminary calculation, a stress of 20 kbar was considered; a fiber will buckle with a pulse longer than 7.8×10^{-3} μsec under these conditions. This is much shorter than the pulse lengths involved in this study. However, a fiber bundle will buckle with a pulse longer than 0.25 μsec under these conditions. This is in the pulse width range of the study. Buckling pulse widths were calculated for fiber bundles for the stress range of the experiments; these are plotted in Figure C-11. If the column is assumed to be pin-ended, the critical load for buckling is given by:

$$P_{crit} = \frac{\pi^2 EI}{L^2} .$$

This expression was also used to calculate critical pulse widths for fiber bundles and the data is also shown in the figure. Comparison of the values from the buckling calculations with the experimental and computer model data show that although buckling of the fiber bundles may contribute to the specimen failure, it does not explain completely the behavior of the material. Further investigation of buckling phenomena was concluded to be beyond the scope of this study.

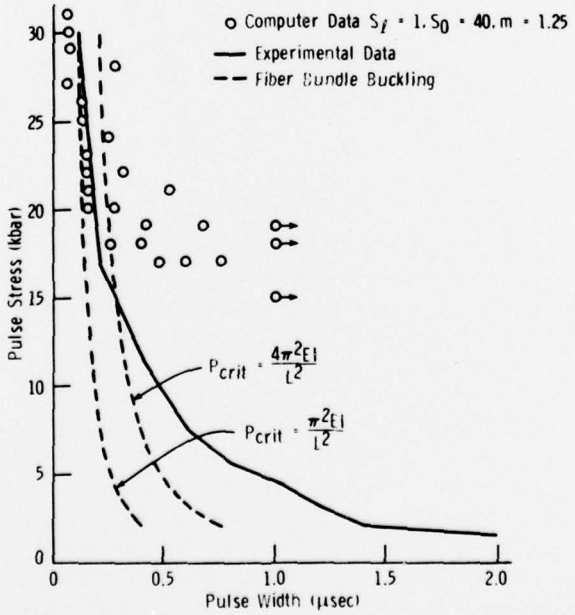

Figure C-11. Comparison of buckling calculations.

APPENDIX D. COMPUTER PROGRAM FOR FIRST MODEL

```
BELT.LI DUMMY
ELT0T7 RLI870 11/21-13:13:42-(,0)
000   C      FIBER BUNDLE FRACTURE UNDER STRESS WAVES
000          REAL RLINE(100),Y(105)
000          REAL WS(200,100),SC(100),SF(100),SFSTOR(100),SWNF(100)
000          REAL WSPR(100,100)
000          INTEGER IFRCT(100), KWSMAX(200)
000          INTEGER F(200)
000          INTEGER IWT(200,100)
000          INTEGER TITLE(20),INT(100)
000          DATA BL/' '/
000          DATA DASH/'-'/
000          DATA X/'X'/
000          IR = 5
000          IW = 6
000          READ(IR,6) NSETS
000   6      FORMAT(10X,I4)
000          DO 999 NSET = 1,NSETS
000          IF(NSET.GT.1)  GO TO 8
000          READ(IR,7) IRAND
000   7      FORMAT(10X,I10)
000   8      CONTINUE
000          READ(IR,9)  (TITLE(I),I = 1,20)
000   9      FORMAT(20A4)
000          READ(IR,10)  ITMAX, JXMAX, IFMAX, RNU, SP, SL, SO, RM, NDEBUG
000   10     FORMAT(3(10X,I4,6X)/2(10X,F10.4)/3(10X,F10.4)/10X,I4)
000          WRITE(IW,20) (TITLE(I),I = 1,20)
000   20     FORMAT(1H1,40H  STRESS WAVE FRACTURE OF FIBER BUNDLES ,
000         1  10H D. DILLEY,14H SEPT.10,1974 /1H ,
000         2  40H  M.S. THESIS MIT DEPT OF MECH ENG        //1H ,20A4)
000          WRITE(IW,22) ITMAX, JXMAX, IFMAX, RNU, SP, SL, SO, RM, IRAND, NDEBUG
000   22     FORMAT(1H ,35H  SAMPLE AND MATERIAL PARAMETERS     /1H ,
000         1  10H    ITMAX =,I4,10H    JXMAX =,I4,10H    IFMAX =,I4/1H ,
000         2  10H      RNU =,F10.4,10H       SP =,F10.4/1H ,
000         3  35H STATISTICS AND CONTROL PARAMETERS /1H ,10H       SL =/F10.4,
000         4  10H       SO =,F10.4,10H       RM =,F10.4/1H ,10H   IRAND =,I10,
000         5  10H  NDEBUG =,I4)
000   C      ZERO THE ARRAY OF WAVE SOURCE STRENGTHS AND SET STRESS PULSE
000          DO 30 JX = 1,JXMAX
000          SF(JX) = SP
000          INT(JX) = JX
000   30     CONTINUE
000          JXMAXT = 2*JXMAX
000          DO 31 K=1,JXMAXT
000          DO 32 KWS=1,JXMAX
000          WS(K,KWS) = 0
000   32     CONTINUE
000   31     CONTINUE
000          DO 311 JXP = 1, JXMAX
000          DO 312 IWTT = 1, ITMAX
000          WSPR(JXP,IWTT) = 0
000   312    CONTINUE
000   311    CONTINUE
000   C CALCULATE FIBER STRENGTH DISTRIBUTION
000          ONEBRM = 1./RM
000          SOMSL = SO -SL
000          Y(1) = IRAND
000          CALL RANDU(Y,JXMAX)
000          IRAND = Y(JXMAX)* 1000000000
000          DO 34 JX = 1, JXMAX
000          SC(JX) = SL + SOMSL * (-ALOG(1.-Y(JX)))**ONEBRM
000   34     CONTINUE
000          WRITE(IW,170)
000   170    FORMAT(1H0,30H SWNF = (.125/(1-RNU))*((1+FAC2NU/(RNMS*RNMS))/RNMS-
000         1 (1+FAC2NU/(RNPS*RNPS))/RNPS)  /1H0,30H FAC2NU = (1-2*RNU)/4     )
000   C  WRITE FIBER STRENGTH DISTRIBUTION
000          WRITE(IW,100)
000   100    FORMAT(1H0,20H  FIBER POSITION  JX/1H0,20H  FIBER STRENGTH  SC//
000         1  1H ,30(4H----))
000          LMAX = (JXMAX-1)/20 + 1
000          DO 35 L = 1,LMAX
000          JBEG = 20*(L-1) + 1
```

```
0000 71      000          JEND = 20*L
000072       000          IF(JEND.GT.JXMAX)  JEND = JXMAX
0000 73      000          WRITE(IW,101)  (INT(JX), JX = JBEG,JEND)
000074       000          JBEG = 20*(L-1) + 1
0000 75      000          JEND = 20*L

000076       000          IF(JEND.GT.JXMAX)  JEND = JXMAX

0000 77      000          WRITE(IW,101)  (INT(JX), JX = JBEG,JEND)

000078       000          JBEG = 20*(L-1) + 1

0000 79      000          JEND = 20*L

000080       000          IF(JEND.GT.JXMAX)  JEND = JXMAX

0000 81      000          WRITE(IW,101)  (INT(JX), JX = JBEG,JEND)
000082       000     101  FORMAT(1HO,20(2X,I4))
0000 83      000          WRITE(IW,102)  (SC(JX), JX = JBEG,JEND)
000084       000     102  FORMAT(1HO,20(1X,F5.1))
0000 85      000          WRITE(IW,105)
000086       000     105  FORMAT(1HO,30(4H****))
0000 87      000     35   CONTINUE
000088       000     C  CALCULATE SOURCE INFLUENCE COEFFICIENTS
0000 89      000          DO 361 NF = 1,ITMAX
000090       000          RNM5 = FLOAT(NF) - .5
0000 91      000          RNP5 = RNM5 + 1.
000092       000          FAC2NU = (1.-2.*RNU)/4.
0000 93      000          SWNF(NF) = (.125/(1.-RNU))*((1.+FAC2NU/(RNM5*RNM5))/RNM5-
000094       000         1  (1. + FAC2NU/(RNP5*RNP5))/RNP5)
0000 95      000     361  CONTINUE
000096       000          IF((JXMAX.GT.20).OR.(NDEBUG.LT.3)) GO TO 36
0000 97      000          WRITE(IW,100)  (SWNF(NF), NF=1,19)
000098       000     100  FORMAT(1HO,20(F5.4))
0000 99      000     C  WRITE CURRENT STRESS ON FIBER ARRAY
000100       000          WRITE(IW,103)
0001 01      000     103  FORMAT(1H1,25H   CURRENT STRESS ARRAY  /1HO,
000102       000         1  20H  FIBER POSITION  JX/1HO,30H  CURRENT STRESS ON FIBER  SF /
0001 03      000         2  /1H ,30(4H****))
000104       000          WRITE(IW,101)  (INT(JX),JX = 1,JXMAX)
0001 05      000     36   CONTINUE
000106       000     C          MAIN CALCULATION
0001 07      000          DO 362  JX=1,JXMAX
000108       000          F(JX) = JX
0001 09      000          F(JX+JXMAX) = JX + JXMAX
000110       000          IFRCT(JX) = 0
0001 11      000     362  CONTINUE
000112       000          DO 363 K = 1, JXMAXT
0001 13      000          KWSMAX(K) = 0
000114       000     363  CONTINUE
0001 15      000          ISUMF = 0
000116       000     C    TIME AND POSITION LOOP - SUM STRESS ARRIVING ALONG CHARACTERISTICS
0001 17      000          DO 60 IT = 1, ITMAX
000118       000          DO 50 JX = 1, JXMAX
0001 19      000     C   CONSIDER EACH CHARACTERISTIC - LEFT AND RIGHT
000120       000          WST = 0
0001 21      000          DO 41 IDRCT = 1,2
000122       000          JXT = JX + JXMAX*(IDRCT-1)
0001 23      000          K = F(JXT)
000124       000          IF(IT.EQ.1) GO TO 41
0001 25      000          KWSMXT = KWSMAX(K)
000126       000          IF(KWSMXT.EQ.0) GO TO 41
0001 27      000          DO 39 KWS = 1,KWSMXT
000128       000          IDT = IT - IWT(K,KWS)
0001 29      000          SDT = SWNF(IDT) * WS(K,KWS)
000130       000          IF(IFRCT(JX).EQ.0) SF(JX) = SF(JX) + SDT
0001 31      000          IF(IFRCT(JX).EQ.1) WST = WST + SDT
000132       000     39   CONTINUE
0001 33      000     41   CONTINUE
000134       000          IF(IFRCT(JX).EQ.0) GO TO 411
0001 35      000          IF(WST.EQ.0) GO TO 411
000136       000          KWSMAX(K) = KWSMAX(K) +1
0001 37      000          KWSNS = KWSMAX(K)
000138       000          WS(K,KWSNS) = WST
0001 39      000          IWT(K,KWSNS) = IT
```

```
000140  000          K = F(JX)
000141  000          KWSMAX(K) = KWSMAX(K) +1
000142  000          KWSNS = KWSMAX(K)
000143  000          WS(K,KWSNS) = WST
000144  000          IWT(K,KWSNS) = IT
000145  000    411   SFSTOR(JX) = SF(JX)
000146  000    C COUNT ANY FIBER FRACTURE AND NUCLEATE A STRESS WAVE
000147  000          IF(SF(JX).LE.SC(JX)) GO TO 50
000148  000          KWSMAX(K) = KWSMAX(K) + 1
000149  000          KWSMXT = KWSMAX(K)
000150  000          WS(K,KWSMXT) = SF(JX)
000151  000          IWT(K,KWSMXT) = IT
000152  000          K = F(JX)
000153  000          KWSMAX(K)=KWSMAX(K)+1
000154  000          KWSMXT=KWSMAX(K)
000155  000          WS(K,KWSMXT)=SF(JX)
000156  000          IWT(K,KWSMXT)=IT
000157  000          ISUMF = ISUMF + 1
000158  000          IFRCT(JX) = 1
000159  000          SF(JX) = 0
000160  000    50    CONTINUE
000161  000          IF((JXMAX.GT.20) .OR.(NDEBUG.LT.7)) GO TO 58
000162  000          WRITE(IW,104) IT, (SFSTOR(JX),JX = 1,JXMAX)
000163  000    104   FORMAT(1HO,10HTIME  IT =,1X,I4/1HO,20(1X,F5.1))
000164  000    58    IF(ISUMF.GE.IFMAX)  ITFAIL = IT
000165  000          IF(ISUMF.GE.IFMAX)  GO TO 87
000166  000    C  ASSIGN NEW CHARACTERISTIC NUMBER TO EACH POSITION
000167  000          JXMAXT = JXMAX-2
000168  000          FTR = F(JXMAX)
000169  000          FTL = F(JXMAX+1)
000170  000          F(JXMAX) = F(JXMAX-1)
000171  000          DO 59 JX = 1,JXMAXT
000172  000          F(JXMAX-JX) = F(JXMAX-JX-1)
000173  000          F(JX+JXMAX) = F(JX+JXMAX+1)
000174  000    59    CONTINUE
000175  000          F(JXMAX+JXMAX-1) = F(JXMAX+JXMAX)
000176  000          F(1) = FTL
000177  000          F(JXMAX+JXMAX) = FTR
000178  000    60    CONTINUE
000179  000    C  END CALCULATIONS
000180  000    C  WRITE ARRAYS AND OTHER DATA. FIRST WAVE SOURCE STRENGTH ARRAY
000181  000          ITFAIL = ITMAX
000182  000    87    CONTINUE
000183  000          DO 642 IT=1,ITFAIL
000184  000          JXMAXP = JXMAX + IT - 1
000185  000          DO 64 K=1,JXMAXP
000186  000          KWSMXT = KWSMAX(K)
000187  000          IF(KWSMXT.EQ.0) GO TO 64
000188  000          DO 641 KWS = 1, KWSMXT
000189  000          IWTT = IWT(K,KWS)
000190  000          JXP = K+IWTT -1
000191  000          IF(K.GT.JXMAX) JXP = IWTT + JXMAX - K
000192  000          IF(JXP.GT.JXMAX) GO TO 641
000193  000          IF(JXP.LT.1) GO TO 641
000194  000          WSPR(JXP,IWTT) = WS(K,KWS)
000195  000    641   CONTINUE
000196  000    64    CONTINUE
000197  000    642   CONTINUE
000198  000          IF(NDEBUG.LT.2)  GO TO 65
000199  000          LMAX = (JXMAX - 1)/20 + 1
000200  000          DO 65 L = 1,LMAX
000201  000          JBEG = 20*(L-1) + 1
000202  000          JEND = 20*L
000203  000          IF(JEND.GT.JXMAX)  JEND = JXMAX
000204  000          WRITE(IW,120)  (INT(JX),JX = JBEG,JEND)
000205  000    120   FORMAT(1H1,3CH WAVE SOURCE STRENGTH ARRAY   /1HO,3C(4H****)//1HO,
000206  000         1  20H  FIBER POSITION  JX/1H/,20(2X,I4))
000207  000          WRITE(IW,122)
000208  000    122   FORMAT(1HO,25H WAVE SOURCE STRENGTH  WS)
000209  000          DO 63 IWTT = 1,ITFAIL
000210  000          WRITE(IW,121) IWTT,(WSPR(JXP,IWTT), JXP=JBEG,JEND)
000211  000    121   FORMAT(1HO,12HTIME IWT  = ,I4/1H ,10(E10.4)/10(E10.4))
000212  000    63    CONTINUE
```

```
000213      COC          DO 643 KWS = 1,20
000214      000          WRITE(IW,123) KWS,(WS(K,KWS), K=JBEG,JEND)
000215      COC    123   FORMAT(1HO,13H SOURCE KWS =,I4/1H ,10(E10.4)/10(E10.4))
000216      000    643   CONTINUE
000217      COC    65    CONTINUE
000218      000    66    CONTINUE
000219      COC          WRITE(IW,20) (TITLE(I),I=1,20)
000220      000          WRITE(IW,22) ITMAX,JXMAX,IFMAX,RNU,SP,SL,SO,RM,IRAND,NDEBUG
000221      COC    C  FIBER BREAK LOCATION FLOTS - 1 FOR EVERY 100 JX
000222      000          LMAX = (JXMAX-1)/100 + 1
000223      COC          DO 75 L = 1,LMAX
000224      000          JBEG = 100*(L-1) + 1
000225      000          JEND = 100*L
000226      000          IF(JEND.GT.JXMAX)  JEND = JXMAX
000227      000    C  WRITE JX EVERY 5 COLUMNS AS A HEADING
000228      000          MMAX = (JEND-JBEG)/5 + 1
000229      000          DO 70 M = 1,MMAX
000230      000    70    INT(M) = 5*M + (L-1)*100
000231      000          WRITE(IW,130)  (INT(M), M = 1,MMAX)
000232      COC    130   FORMAT(1HO,30H BROKEN FIBER POSITION   JX    /1HO,10X,20I5)
000233      000    C  BLANK ALL COLUMNS
000234      COC          DO 71 N = 1,100
000235      000    71    RLINE(N) = BL
000236      COC          DO 73 IT = 1,ITFAIL
000237      000          DO 72 J = JBEG,JEND
000238      COC          N = J - JBEG + 1
000239      000    C SET AND RETAIN X FOR BROKEN FIBERS (DASH FOR UNBROKEN)
000240      000          IF((NSPR(J,IT).NE.0).OR.(RLINE(N).EQ.X)) RLINE(N) = X
000241      000          IF(RLINE(N).NE.X) RLINE(N)  = DASH
000242      COC    72    CONTINUE
000243      000    C WRITE FRACTURE SYMBOLS FOR ALL IT (LABEL IT EVERY 5)
000244      COC          IF(MOD(IT,5).NE.0)  GO TO 74
000245      000          WRITE(IW,131) IT, (RLINE(N), N=1,100)
000246      COC    131   FORMAT(1H ,4HIT =,I4,2X,100A1)
000247      000          GO TO 73
000248      COC    74    WRITE(IW,132) (RLINE(N), N=1,100)
000249      000    132   FORMAT(1H ,10X,100A1)
000250      COC    73    CONTINUE
000251      000    75    CONTINUE
000252      COC          WRITE(IW,140)  ITFAIL
000253      000    140   FORMAT(1HO,10H ITFAIL = ,I4)
000254      COC    999   CONTINUE
000255      000          STOP
000256      COC          END

END OF F.

/EOR

/EOF
```

APPENDIX E. COMPUTER PROGRAM FOR SECOND MODEL

```
C     FIBER BUNDLE FRACTURE UNDER STRESS WAVES
      REAL SW(99,100),SC(100),SF(100),SFSTOR(100),RLINE(100),SWNF(100)
      INTEGER TITLE(20),INT(100)
      DATA BL/' '/
      DATA DASH/'-'/
      DATA X/'X'/
      IR = 5
      IW = 6
      READ(IR,6) NSETS
6     FORMAT(10X,I4)
      DO 999 NSET = 1,NSETS
      IF(NSET.GT.1)  GO TO 8
      READ(IR,7) IRAND
7     FORMAT(10X,I10)
8     CONTINUE
      READ(IR,9) (TITLE(I),I = 1,20)
9     FORMAT(20A4)
      READ(IR,10)  ITMAX,JXMAX,IFMAX,RNU,SP,SL,S0,RM,NDEBUG
10    FORMAT(3(10X,I4,6X)/2(10X,F10.4)/3(10X,F10.4)/10X,I4)
      WRITE(IW,20) (TITLE(I),I=1,20)
20    FORMAT(1H1,40H  STRESS WAVE FRACTURE OF FIBER BUNDLES ,
     1  10H E. CILLEY,14H JAN.6,1974   /1H ,
     2  40H  M.S. THESIS MIT DEPT OF MECH ENG      //1H ,20A4)
      WRITE(IW,22) ITMAX,JXMAX,IFMAX,RNU,SP,SL,S0,RM,IRAND,NDEBUG
22    FORMAT(1H ,35H  SAMPLE AND MATERIAL PARAMETERS   ,/1H ,
     1  10H   ITMAX =,I4,10H   JXMAX =,I4,10H   IFMAX =,I4/1H ,
     2  10H     RNU =,F10.4,10H      SP =,F10.4/1H ,
     3  35H STATISTICS AND CONTROL PARAMETERS /1H ,10H      SL =,F10.4,
     4  10H       S0 =,F10.4,10H      RM =,F10.4/1H ,10H   IRAND =,I10,
     5  10H  NDEBUG =,I4)
C     ZERO THE ARRAY OF WAVE SOURCE STRENGTHS AND SET STRESS PULSE
      DO 30 JXW = 1, JXMAX
      SF(JXW) = SP
      INT(JXW) = JXW
      DO 30 ITW = 1, ITMAX
30    SW(ITW,JXW) = 0
C  CALCULATE FIBER STRENGTH DISTRIBUTION
      READ(IR,200) (SC(JX),JX=1,JXMAX)
200   FORMAT(10(2X,F5.1),10X)
34    CONTINUE
C  FIBER STRENGTH DISTRIBUTION
      WRITE(IW,100)
100   FORMAT(1H0,20H  FIBER POSITION  JX/1H0,20H  FIBER STRENGTH  SC//
     1  1H ,30(4H****))
      LMAX = (JXMAX-1)/20 + 1
      DO 35  L = 1,LMAX
      JBEG = 20*(L-1) + 1
      JEND = 20*L
      IF(JEND.GT.JXMAX)  JEND = JXMAX
      WRITE(IW,101)  (INT(JX), JX = JBEG,JEND)
101   FORMAT(1H0,20(2X,I4))
      WRITE(IW,102)  (SC(JX), JX = JBEG,JEND)
102   FORMAT(1H0,20(1X,F5.1))
      WRITE(IW,105)
105   FORMAT(1H0,30(4H****))
35    CONTINUE
      WRITE(IW,150)  IRAND
150   FORMAT(1H0,10H  IRAND = ,I10)
$PRINTON
      WRITE(IW,160)
160   FORMAT(1H0,80H  SWNF = (.125/(1-RNU))*((1+FAC2NU/(RNM5*RNM5))/RNM5
     1-(1+FAC2NU/(RNP5*RNP5))/RNP5 )
C      CURRENT STRESS ON FIBER ARRAY
      IF(JXMAX.GT.20)  GO TO 36
      WRITE(IW,103)
```

```
103   FORMAT(1H1,25H   CURRENT STRESS ARRAY  /1H0,
     1  20H  FIBER POSITION  JX/1H0,30H  CURRENT STRESS ON FIBER  SF /
     2  /1H ,30(4H****))
      WRITE(IW,101)  (INT(JX),JX = 1,JXMAX)
36    CONTINUE
C  CALCULATE SOURCE ARRAY VALUES
      DO 361 NF = 1, ITMAX
      RNM5 = FLOAT(NF) - .5
      RNP5 = RNM5 + 1.
      FAC2NU = (1. - 2. *RNU)/32.
      SNNF(NF) = (.125/(1.-RNU))*((1.+FAC2NU/(RNM5*RNM5))/RNM5-
     1  (1. + FAC2NU/(RNP5*RNP5))/RNP5)
361   CONTINUE
C  BEGIN TIME LOOP
      DO 60 IT = 1, ITMAX
      ISUMF = 0
      DO 50 JX = 1, JXMAX
      IF(IT.EQ.1) GO TO 41
C  SET FRACTURE INDEX FOR BROKEN FIBERS AND SUM THEM
      IFRCT = 0
      IF(SF(JX).NE.0.) GO TO 37
      ISUMF = ISUMF + 1
      IFRCT = 1
C  DEFINE WAVES FROM SOURCES AFFECTING THE PRESENT IT AND JX
37    ITWMAX = IT - 1
      DO 40 ITW  = 1, ITWMAX
      DO 39 JXW = 1,JXMAX
      SWIJW = SW(ITW,JXW)
      IF(SWIJW) 371,39,371
371   NF = IT - ITW
      IF(NF-IABS(JX-JXW)) 383,385,383
383   IF(NF-(JXMAX-JXW+JXMAX-JX+1)) 386,385,386
386   IF(NF-(JXW-1+JX)) 39,385,39
C  FIND STRESS INCREMENT ON FIBER JX, EMIT IT FROM BROKEN FIBER
385   SDT = SWIJW*SNNF(NF)
      IF(NF-IABS(JX-JXW)) 387,389,387
387   IF(JXMAX-JXW+JXMAX-JX+1-JXW+1-JX) 389,388,389
388   SDT = SDT + SDT
389   IF(IFRCT) 38,391,38
391   SF(JX) = SF(JX) + SDT
      GO TO 39
38    SW(IT,JX) = SW(IT,JX) + SDT
39    CONTINUE
40    CONTINUE
41    CONTINUE
      SFSTOR(JX) = SF(JX)
C  COUNT ANY FIBER FRACTURE AND NUCLEATE A STRESS WAVE
      IF(SF(JX).LE.SC(JX))  GO TO 50
      ISUMF = ISUMF + 1
      SW(IT,JX) = SF(JX)
      SF(JX) = 0
50    CONTINUE
C IS SPECIMEN FAILED OR PULSE GONE BY?
      IF(JXMAX.GT.20) GO TO 58
      WRITE(IW,104) IT, (SFSTOR(JX),JX = 1,JXMAX)
104   FORMAT(1H0,10HTIME  IT =,1X,I4/1H0,20(1X,F5.1))
58    IF(ISUMF.GT.IFMAX)  ITFAIL = IT
      IF(ISUMF.GT.IFMAX)  GO TO 67
60    CONTINUE
$PRINTOFF
C  WAVE SOURCE STRENGTH ARRAY
      ITFAIL  = ITMAX
67    CONTINUE
      IF(NDEBUG.GT.2)  GO TO 66
      LMAX = (JXMAX - 1)/20 + 1
      DO 65 L = 1,LMAX
      JBEG = 20*(L-1) + 1
      JEND = 20*L
      IF(JEND.GT.JXMAX)  JEND = JXMAX
      WRITE(IW,120)  (INT(JX),JX = JBEG,JEND)
```

```
120   FORMAT(1H1,30H WAVE SOURCE STRENGTH ARRAY   /1H0,30(4H****)//1H0,
     1  20H  FIBER POSITION  JX/1H/,20(2X,I4))
      WRITE(IW,122)
122   FORMAT(1H0,25H WAVE SOURCE STRENGTH  SW)
      DO 63  ITW = 1, ITFAIL
      WRITE(IW,121) ITW, (SW(ITW,JXW), JXW = JBEG,JEND)
121   FORMAT(1H0,12HTIME  ITW = ,I4/1H ,20(1X,F5.1))
63    CONTINUE
65    CONTINUE
66    CONTINUE
C  FIBER BREAK LOCATION PLOTS - 1 FOR EVERY 100 JX
      LMAX = (JXMAX-1)/100 + 1
      DO 75 L = 1,LMAX
      JBEG = 100*(L-1) + 1
      JEND = 100*L
      IF(JEND.GT.JXMAX)  JEND = JXMAX
C  WRITE JX EVERY 5 COLUMNS AS A HEADING
      MMAX = (JEND-JBEG)/5 + 1
      DO  70  M = 1,MMAX
70    INT(M) = 5*M + (L-1)*100
      WRITE(IW,130)  (INT(M), M = 1,MMAX)
130   FORMAT(1H1,30H  BROKEN FIBER POSITION  JX   /1H0,10X,20I5)
C  BLANK ALL COLUMNS
      DO 71  K = 1,100
71    RLINE(K) = BL
      DO 73 IT = 1,ITFAIL
      DO 72 J = JBEG,JEND
      K = J - JBEG + 1
C  SET AND RETAIN X FOR BROKEN FIBERS (DASH FOR UNBROKEN)
      IF((SW(IT,J).NE.0.).OR.(RLINE(K).EQ.X))  RLINE(K) = X
      IF(RLINE(K).NE.X)  RLINE(K) = DASH
72    CONTINUE
C  WRITE FRACTURE SYMBOLS FOR ALL IT (LABEL IT EVERY 5)
      IF(MOD(IT,5).NE.0)  GO TO 74
      WRITE(IW,131)  IT, (RLINE(K), K = 1,100)
131   FORMAT(1H ,4HIT =,I4,2X,100A1)
      GO TO 73
74    WRITE(IW,132)  (RLINE(K), K = 1,100)
132   FORMAT(1H ,10X,100A1)
73    CONTINUE
75    CONTINUE
      WRITE(IW,140)  ITFAIL
140   FORMAT(1H0,10H ITFAIL = ,I4)
999   CONTINUE
      STOP



      END
```

DISTRIBUTION LIST

No. of Copies	To
1	Office of the Director, Defense Research and Engineering, The Pentagon, Washington, D. C. 20301
12	Commander, Defense Documentation Center, Cameron Station, Building 5, 5010 Duke Street, Alexandria, Virginia 22314
1	Metals and Ceramics Information Center, Battelle Columbus Laboratories, 505 King Avenue, Columbus, Ohio 43201
	Deputy Chief of Staff, Research, Development, and Acquisition, Headquarters Department of the Army, Washington, D. C. 20310
1	ATTN: DAMA-ARZ
	Commander, Army Research Office, P. O. Box 12211, Research Triangle Park, North Carolina 27709
1	ATTN: Information Processing Office
	Commander, U. S. Army Materiel Development and Readiness Command, 5001 Eisenhower Avenue, Alexandria, Virginia 22333
1	ATTN: DRCLDC, Mr. R. Zentner
	Commander, U. S. Army Materiel Systems Analysis Activity, Aberdeen Proving Ground, Maryland 21005
1	ATTN: DRXSY-MP
	Commander, U. S. Army Communications Research and Development Command, Fort Monmouth, New Jersey 07703
1	ATTN: DRDCO-GG-DD
1	DRDCO-GG-DM
	Commander, U. S. Army Missile Research and Development Command, Redstone Arsenal, Alabama 35809
1	ATTN: Technical Library
	Commander, U. S. Army Armament Research and Development Command, Dover, New Jersey 07801
2	ATTN: Technical Library
1	DRDAR-SCM, J. D. Corrie
	Commander, U. S. Army Foreign Science and Technology Center, 220 7th Street, N. E., Charlottesville, Virginia 22901
1	ATTN: Military Tech, Mr. Marley
	Director, U. S. Army Ballistic Research Laboratory, Aberdeen Proving Ground, Maryland 21005
1	ATTN: DRDAR-TSB-S (STINFO)

No. of Copies	To
	Naval Research Laboratory, Washington, D. C. 20375
1	ATTN: Dr. J. M. Krafft - Code 8430
	Chief of Naval Research, Arlington, Virginia 22217
1	ATTN: Code 471
	Air Force Materials Laboratory, Wright-Patterson Air Force Base, Ohio 45433
2	ATTN: AFML/MXE/E. Morrissey
1	AFML/LC
1	AFML/LLP/D. M. Forney, Jr.
1	AFML/MBC/Mr. Stanley Schulman
	National Aeronautics and Space Administration, Washington, D. C. 20546
1	ATTN: Mr. B. G. Achhammer
1	Mr. G. C. Deutsch - Code RW
	National Aeronautics and Space Administration, Marshall Space Flight Center, Huntsville, Alabama 35812
1	ATTN: R. J. Schwinghammer, EH01, Dir, M&P Lab
1	Mr. W. A. Wilson, EH41, Bldg. 4612
1	Mechanical Properties Data Center, Belfour Stulen Inc., 13917 W. Bay Shore Drive, Traverse City, Michigan 49684
	Director, Army Materials and Mechanics Research Center, Watertown, Massachusetts 02172
2	ATTN: DRXMR-PL
1	DRXMR-WD
2	Authors